HHS Public Access

Author manuscript

Biochemistry. Author manuscript; available in PMC 2019 December 10.

Published in final edited form as:

Biochemistry. 2018 November 13; 57(45): 6416–6433. doi:10.1021/acs.biochem.8b00732.

Resonance Raman, EPR and MCD Spectroscopic Investigation of Diheme Cytochrome *c* Peroxidases from *Nitrosomonas europaea* and *Shewanella oneidensis*

Matthew W. Wolf, **Kimberly Rizzolo**, **Sean J. Elliott***, **Nicolai Lehnert***

Department of Chemistry and Department of Biophysics, University of Michigan, Ann Arbor, MI 48109

Department of Chemistry, Boston University, 590 Commonwealth Avenue, Boston, Massachusetts 02215

Abstract

Cytochrome *c* peroxidases (bCcPs) are diheme enzymes required for the reduction of H2O2 to water in bacteria. There are two classes of bCcPs: one class of enzymes is active in the diferric form (constitutively active), and the other class of enzymes requires the reduction of the high-potential heme (H-heme) before catalysis commences (reductively activated) at the low-potential heme (L-heme). In order to better understand the mechanisms and heme electronic structures of these different bCcPs, a constitutively active bCcP from *Nitrosomonas europaea* (*Ne*CcP) and a reductively activated bCcP from *Shewanella oneidensis* (*So*CcP) were characterized in both the diferric and semi-reduced states by electron paramagnetic resonance (EPR), resonance Raman (rRaman), and magnetic circular dichroism (MCD) spectroscopy. In contrast to some previous crystallographic studies, EPR and rRaman spectra do not indicate the presence of significant amounts of a five-coordinate, high-spin ferric heme in *Ne*CcP or *So*CcP in either the diferric or semi-reduced states in solution. This points towards a mechanism of activation where the active site L-heme is not in a static, five-coordinate state, but where the activation is more subtle and likely involves formation of a six-coordinate hydroxo complex, which could then react with hydrogen peroxide in an acid-base type reaction to create Compound 0, the ferric hydroperoxo complex. This mechanism lies in stark contrast to the diheme enzyme MauG that exhibits a static, five-coordinate open heme site at the peroxidatic heme, and that forms a more stable Fe^{IV}=O intermediate.

Graphical Abstract

***Corresponding Author** elliott@bu.edu, lehnertn@umich.edu.

ASSOCIATED CONTENT:

Supporting Information:

The Supporting Information is available free of charge at and contains information on the following: a table of constitutively active and reductively activated bCcPs, MCD spectra of ferric cytochrome b5, oxidized and reduced *Ne*H59G CcP, and oxidized and reduced SoH80G CcP, resonance Raman spectra investigating the power dependence of *Ne*CcP, *So*CcP and their respective mutants, as well as room temperature resonance Raman spectra of all of these enzymes, a fit of the highly rhombic EPR signal of *Ne*H59G CcP, and the EPR spectra of semi-reduced *So*CcP from pH 5.5–9.

Spectroscopic methods are used to interrogate the diferric and semi-reduced forms of bacterial Cyt. *c* peroxidases from *Nitrosomonas europaea* (*Ne*CcP) and *Shewanella oneidensis* (*So*CcP). Our results indicate that the L-heme is not in a static, five-coordinate state in the catalytically active forms of these enzymes, but that the activation mechanism of these enzymes is more subtle, and different from MauG.

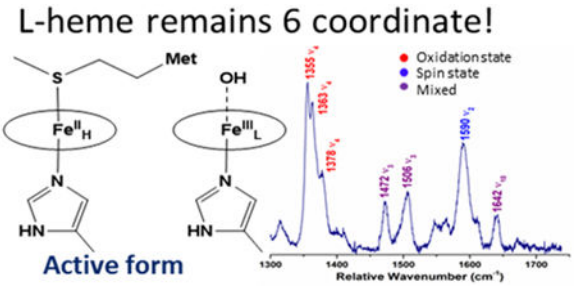

Introduction

Hydrogen peroxide (H_2O_2) is produced as an undesired by-product of the electron transport chain during aerobic respiration and can damage cells through decay into hydroxyl or superoxide radicals.[1] In many gram negative bacteria, excess H_2O_2 is reduced to water by soluble, periplasmic cytochrome *c* peroxidases (bCcPs) in order to avoid the buildup of toxic radical species.[2] Each canonical bCcP is a homodimer, where each protomer contains two covalently-bound, *c*-type heme cofactors in separate domains (Figure 1). One of the hemes exhibits a relatively high $Fe^{III/II}$ redox potential, typically between 330 to 450 mV (vs. NHE).[3–4] This high-potential (H-heme, or Fe_H) is axially coordinated by His and Met residues, and facilitates electron transfer to the active site from small donor proteins. The H-heme also stores reducing equivalents that can be utilized during peroxide reduction.[4–6] The active site is a peroxidatic, low-potential heme (L-heme) where H_2O_2 binds and is reduced to water.[2] The L-heme has a $Fe^{III/II}$ redox potential that ranges in between −330 to −250 mV vs. NHE, like other heme peroxidases.[3–4] Most bCcPs can be referred to as ‘activatable’: while the enzyme rests in the diferric form, it is catalytically inactive,[7] due to the ligation of two His residues at each apical position of the L-heme active site (see Table S1).[6–13] Activation is achieved by reducing the H-heme, producing a stable, ‘semi-reduced’ activated state ($Fe_H^{II}Fe_L^{III}$) where the H-heme is ferrous and the L-heme remains ferric. Most bCcPs belong to this class, and the most well-studied example is the bCcP from *Pseudomonas aeruginosa* (*Pa*CcP). Indeed, x-ray crystal structures of *Pa*CcP or orthologs from *Geobacter sulfurreducens*[14] and *Paracoccus pantotrophus*[8] show that transformation from the asisolated enzyme to the semi-reduced form involves a change of coordination environment at the active site. When fully oxidized (Fe_H^{III} Fe_L^{III}), the six-coordinate (6C) L-heme is ligated by two His residues (one from the canonical CXXCH motif that binds the *c*-type hemej, and that upon reduction of the H-heme ($Fe_H^{II}Fe_L^{III}$), the distal Fe_L-N_{His} bond is broken, creating a presumed five-coordinate (5C) site which allows H_2O_2 to bind to the iron center.[7–8, 15] Spectroscopic data from UV-vis and room temperature near-IR MCD indicate that the L-heme changes spin states from low-spin ferric to high-spin ferric upon semi-reduction at the H-heme.[16–17]

In contrast, the other class of bCcPs is 'constitutively active', meaning that the bCcPs are catalytically competent in both the diferric and semi-reduced states (Table S1).[3, 18] While there are fewer examples of enzymes in this class compared to the 'activatable' class, they include the bCcP from *Nitrosomonas europaea* (*Ne*CcP) which has been characterized by UV-vis and EPR spectroscopy, as well as protein crystallography.[3, 19] The crystal structure of the enzyme has been reported as a 5C L-heme (no water or other exogenous ligand bound) for the as-isolated enzyme, indicating it is ready to bind H2O2.[19] In terms of primary amino acid sequences there are few clues as to what makes a constitutively active bCcP distinct from an activatable enzyme: for example, *Ne*CcP shares high sequence identity (~60%) and high structural homology (RMSD of backbone atoms = 0.455 A)[20] with the bCcP from *Shewanella oneidensis* (*So*CcP), which is a member of the 'activatable' class of bCcPs. Importantly, the His which acts as a ligand to the inert $Fe_H^{III}Fe_L^{III}$ form of all activatable bCcPs is retained in the *Ne* enzyme (and indeed in all proven constitutively active enzymes). Further, while the *Ne* and *So* enzymes catalyze the same reaction, one imagines that by starting a catalytic cycle at different redox states (Scheme 1), that different mechanisms should be at work in the *Ne* and *So* enzymes.[13, 20–21] The catalytic mechanism of *Ne*CcP is proposed to be similar to monoheme peroxidases with H_2O_2 binding to the L-heme and an Fe^{IV}=O $R^{\cdot+}$ "Compound I"-like intermediate with a cation radical located on either the porphyrin ring or an adjacent tryptophan residue. In the second step, reduction to a "Compound II"-like species occurs through a small electron-donor protein such as Cytochrome C551 prior to the formation of a ferrichydroxo species and release of a second equivalent of water. In contrast, it is proposed that "activatable" bCcPs, including *So*CcP, must go through the reduction of the H-heme first before binding H_2O_2 at the L-heme and forming an Fe^{IV}=O Compound II-like intermediate without having to go through a Compound I species.[20]

MauG is also member of the bCcP family, containing the same core-fold and architecture of two *c*-type hemes that are in communication with one another via a conserved Trp residue.[22–23] However, the redox potentials of the two MauG hemes are not well-separated[24] such that an analogous form of the semi-reduced state ($Fe^{III}Fe^{III}$) is impossible; as such, the analogous H-heme is referred to only as the 6C heme, and it contains His/Tyr ligation (instead of His/Met), and the peroxidatic heme is referred to as the 5C heme. Mechanistically, MauG has been associated with the utilization of a unique $Fe^{IV}Fe^{IV}$=O state,[25] which is required for the native function of MauG (the six-electron oxidation of the precursor protein of methylamine dehydrogenase, in order to install the tryptophanyl-tryptophanequinone (TTQ) cofactor).

Rationalizing the distinct redox states, spectroscopic properties and mechanistic details of the bCcP family has proven challenging: For example, while the peroxidatic heme of MauG is clearly 5C (determined by not only crystallography but also spectroscopy[22–24]) the same coordination environment at the active site of activated, canonical bCcP has yet to be established through spectroscopic means. We posit that the differences between MauG and canonical bCcPs are tied to these differences in the relative stabilization of 5C and 6C states, and the resultant redox potentials of the two hemes. Thus, evaluating the coordination chemistry and spin-state(s) of the peroxidative active site in bCcPs is an essential missing piece of our understanding of these enzymes. In this paper, we use EPR, resonance Raman

(rRaman) and MCD spectroscopy to evaluate whether or not canonical bCcPs, when active, do indeed produce a true 5C form at the active site. Here we use the constitutively active *N. europaea* enzyme and the activatable *S. oneidensis* enzymes as model systems to compare the spectroscopic traits with known differences in enzymatic activity. Single point mutation variants of *Ne*CcP and *So*CcP (H59G and H80G, respectively) were also prepared to remove the native distal His residue that can coordinate to the L-heme. The spectra of the native protein and the variants that lack the distal His could then be compared to help assign the oxidation and spin states of the catalytically-relevant L-heme. Spectroscopic data were collected on both the diferric and semi-reduced forms of each of these enzymes and analyzed in detail.

Experimental Procedures

Protein Expression and Purification of wt *So* and H80G.

Expression and purification of wild-type (wt) *So* and the H80G variant was performed as described previously.[13, 20] For semi-reduced samples, *So* samples were incubated on ice for 1.5 hr in the presence of 2 mM sodium ascorbate and 1 mM diaminodural. For oxidized samples, *So* was incubated with 1 mM hexachloroiridate on ice for 1.5 hr. The semi-reduced and oxidized states of *So* and H80G were verified by collecting their absorption spectra on a Cary50 UV-Vis spectrophotometer (Agilent). Final samples were exchanged into 100 mM TIP7 buffer with 30% glycerol before storing at −80°C until use. For pH dependent EPR studies, semi-reduced wt So samples were prepared in 50 mM MES, 100 mM NaCl, pH 5.5 and 50 mM TAPS, 100 mM NaCl, pH 9.0. Optical spectra verified semi-reduced state before collecting EPR spectra.

Protein Expression and Purification of wt *Ne* and H59G.

The *Ne* gene was removed from the pMAL-Tev-*Ne*CcP vector as previously described[20] by PCR with overhang ends that anneal outside the N-terminal Strep tag and C-terminal 6x-His tag of the pETSN vector.[12] PCR was carried out using Platinum High-Fidelity Super mix (Invitrogen) with the following primers: 5'-TTCGCTACCGTAGCGCAGGCCGGTAGTGGCAATGAACCGATACAACCG (forward) and 5'-GGGCTTTGTTAGCAGCCGGATCTTACTCATACGGCTGAGAACGTGGTGTATC (reverse). The amplified PCR product was gel purified and used as the megaprimer in a QuikChange reaction with the pETSN vector as template (QuikChange Lightning II kit, Agilent). Insertion of the *Ne* gene was verified by sequencing (GeneWiz). *Ne-pETSN2* was co-transformed with a plasmid containing the Cytochrome *c* maturation cassette[26] into BL21(DE3) competent cells. Starter cultures of 5 mL were grown overnight at 37°C in 2x YT, supplemented with 100 μg/mL ampicillin and 35 μg/mL chloramphenicol. The culture was harvested and resuspended in fresh media before inoculating it in a 1L flask of 2x YT for bulk expression at 37°C with 220 rpm until $0D_{600}$=0.8 was reached. Cells were cooled and induced with 400 μM β-d-thiogalactopyranoside (IPTG, Bio-rad) for 17 hrs at room temperature with shaking at 150 rpm. Cell pellets were harvested by centrifugation, resuspended in 20 mM Tris, 1 mM PMSF, pH 8.2, and lysed by sonication. The lysate was clarified by centrifugation and the supernatant was loaded onto a Q-Sepharose anion exchange resin (GE) equilibrated with lysis buffer. The bound protein was washed

extensively with 20 mM Tris, 20 mM NaCl, pH 8.2 before elution at 40 mM NaCl. Pooled fractions were concentrated in Amicon 30K MWCO and loaded onto a S-200 size exclusion column (GE) equilibrated in 50 mM HEPES, 100 mM NaCl, pH 7.8. Pure fractions were concentrated and exchanged into TIP7 buffer. The histidine residue at position 59 in *Ne* was mutated to a glycine using the QuikChange Lightning Mutagenesis Kit with the following primers: 5'-CGATAATATTACCACCTCGATCGGGGGCAAATGGCAGCAAGGCCCGATCAATGC (forward) and 5'-GACTTGATCGGGCCTTGCTGCCATTTGCCCCCGATCGAGGTGGTAATATTATCG (reverse). For semi-reduced samples, *Ne* protein samples were incubated on ice for 1.5 hr in the presence of 2 mM sodium ascorbate (Sigma) and 1 mM diaminodural. For oxidized samples, *Ne* was incubated with 1 mM hexachloroiridate on ice for 3 hr. The semi-reduced and oxidized states of *Ne* and H59G were verified by collecting their absorption spectra on a Cary50 UV-Vis spectrophotometer (Agilent). Final samples were exchanged into 100 mM TIP7 buffer with 30% glycerol before storing at −80°C until use.

Preparation of myoglobin and cytochrome *c*.

Horse heart myoglobin and horse heart cytochrome *c* were purchased from Sigma-Aldrich. Horse heart cytochrome *c* was oxidized with excess potassium ferricyanide, purified on a Sephadex G-25 column, and concentrated prior to use. To prepare ferrous cytochrome *c*, excess sodium ascorbate was added and the protein was allowed to briefly incubate on ice before freezing in liquid nitrogen.

EPR Spectroscopy.

Electron paramagnetic resonance spectra were measured on a Bruker X-Band EMX spectrometer equipped with an Oxford Instruments 3 S3 liquid helium cryostat. EPR spectra were obtained on frozen solutions using 20 mW microwave power and 100 kHz field modulation with the amplitude set to 1 G. All samples were measured at 12 K.

Resonance Raman Spectroscopy.

Most Raman spectra were recorded in 3 mm diameter EPR tubes. Typical sample concentrations range from 0.1 to 0.16 mM. A SpectraPhysics BeamLok 2060-RS Krypton ion gas laser was used for excitation of the samples at 413.1 nm. The scattered light from the samples was focused onto an Acton two-stage TriVista 555 monochromator and detected by a liquid N_2-cooled Princeton Instruments Spec-10:400B/LN CCD camera. Data were collected at liquid nitrogen temperature using an EPR cold finger to cool the samples, and at room temperature using an NMR spinner powered with compressed air. Typical laser powers were in the 15–30 mW range, and a spectral resolution of 0.3 cm^{-1} was used. The room temperature semi-reduced spectra were obtained with 407 nm excitation by a tunable titanium :sapphire laser (Spectra-Physics Tsunami) pumped by a 25 W DPSS laser (Spectra-Physics Millennia eV) and configured with a 10 ps Gires–Tournois interferometer. These samples were not rotated with an NMR spinner; instead lower laser power in the range of 4–8 mW was used (Shafaat laboratory, Ohio State University).

Magnetic Circular Dichroism Spectroscopy.

Protein samples were prepared in 50 mM TIP7 buffer with 50–60% glycerol (a glassing agent) added to each sample. Typical sample concentrations range from 5 μM to 20 μM, depending on the spectral region of interest. Samples were placed between two quartz plate windows in an MCD sample holder. The samples were frozen in liquid nitrogen until a transparent glass formed. The MCD setup is comprised of an OXFORD SM4000 cryostat and a JASCO J-815 CD spectrometer. The SM4000 cryostat consists of a liquid helium-cooled superconducting magnet providing horizontal magnetic fields of 0–7 T. The J-815 spectrometer uses a gaseous nitrogen-cooled xenon lamp and a detector system with two interchangeable photomultiplier tubes in the UV-vis and NIR range. The samples were loaded into a 1.5–300 K variable temperature insert (VTI) which allows optical access to the sample via four optical windows made from Suprasil B quartz. The MCD spectra were measured in [θ] = mdeg and manually converted to $\Delta\varepsilon$ ($M^{-1}cm^{-1}T^{-1}$) using the conversion factor $\Delta\varepsilon = \theta/(32980\ cdB)$ were c is the concentration, B is the magnetic field, and d is the path length. The product cd can be substituted by $A_{MCD}/\varepsilon UV_{-vis}$, where A is the absorbance of the sample measured by the CD spectrometer.[27] Complete spectra were recorded at different temperatures (2, 5, and 10 K) and magnetic fields (0, 1, 3, 5, and 7 T). For the photolysis experiments, a mercury lamp was used as a light source to illuminate the samples for 15 min before re-measuring the samples.

Results & Analysis

MCD Benchmark Studies

MCD spectra of high-spin ferric myoglobin (metMb), low-spin ferric Cytochrome (Cyt.) b_5, and both low-spin ferric and ferrous Cyt. c were taken in order to compare these benchmark spectra to the spectra of *Ne*CcP and *So*CcP. The heme in metMb is coordinated by the proximal His and a weakly-bound water molecule at pH 7. MetMb exhibits a positive band in the Soret region at 24830 cm^{-1} and a negative feature at 23300 cm^{-1} (Figure 2a). Less intense bands closer to the Q-band region of the heme are also present at 22280 and 20640 cm^{-1}, and in the 18770 to 15660 cm^{-1} region. In comparison, the Soret band MCD features of the high-spin ferric heme in metMb are much less intense (by an order of magnitude) compared to the corresponding features of the low-spin ferric hemes in Cyt. b_5 and Cyt. c (see Figures S1 and 2b), as expected.[27–31] In Cyt. b_5, the heme is coordinated by two axial His ligands. The MCD spectrum of Cyt. b_5 exhibits a positive Soret feature at 24560 cm^{-1} and a negative band at 23920 cm^{-1}. Weaker Q-band signals are present at 22220, 20810, 18440, 17830, and 17160 cm^{-1}. Cyt. c is coordinated by one His and one Met residue, but exhibits a very similar MCD spectrum to Cyt. b_5 in the low-spin ferric state (Figure 2b). In the Soret region, bands are present at 24870 cm^{-1} and 24100 cm^{-1}, and less intense Q-band features are observed at 22000, 20710, 18360, and 17810 cm^{-1}. The spectra for both Cyt. b_5 and Cyt. c are very typical for low-spin ferric hemes.[30] In contrast to this, low-spin ferrous Cyt. c is diamagnetic and exhibits only a very weak feature in the Soret region at 24070 cm^{-1} (Figure 2c). A more intense MCD **A**-term signal that does not vary in intensity with changes in temperature is present at 18270 cm^{-1}, which is assigned to the Q-band. To higher energy of the Q-band, smaller diamagnetic signals are observed at 19920, 19570, 19310, and 18730 cm^{-1}, which are vibronic in nature and assigned to the Q_v band.[32]

EPR Spectra of Ne*CcP* (constitutively active)

EPR spectra were taken at 12 K for both the wild-type (wt) *Ne*CcP and the H59G mutant of the enzyme (*Ne*H59G CcP), where the distal His of the L-heme has been removed. Diferric *Ne*CcP exhibits an anisotropic low-spin signal at g = 3.41 that completely disappears upon reduction (Figures 3a and b). This signal must result from the H-heme, which is reduced to the ferrous state in the presence of ascorbate.[13] Note that the H-heme therefore belongs to the class of "large g_{max}" low-spin ferric hemes, which generally only show one resonance in their EPR spectra. "Large g_{max}" signals usually arise when hemes exhibit a bis-His coordination or a His/Met coordination, and the two axial ligands are perpendicular to one another.[33,34] The L-heme exhibits dominant low-spin signals at g = 2.91, 2.41, and 1.50 at 12 K (Figure 3b). A very small amount of a putative high-spin ferric species is also present that shows a signal at g = 6.15, which we tentatively assign to a small fraction of the L-heme that is in the high-spin state. The EPR spectra of the mutant, *Ne*H59G CcP, exhibit a similar signal for the H-heme at g = 3.40, and for the low-spin ferric L-heme at 2.90, 2.41, and 1.57. The putative high-spin component is also present with a signal at g = 6.13, again in a very small concentration. It is interesting to note that the ferric L-heme shows very similar EPR parameters in wt enzyme and the H59G mutant (which lacks the distal His), indicating that the L-heme in wt enzyme does not correspond to a bis-His site either. In both cases, the L-heme is either able to attract another amino acid side chain as a ligand, or potentially a water/hydroxide molecule, or maybe a mixture of these two possibilities, resulting in a low-spin complex. In addition to this, the spectra for *Ne*H59G CcP exhibit signals at g = 4.82, 4.09, and 3.78 which originate from a very rhombic ($E/D \sim 0.28$), high-spin ferric species (see Figure S14). This form of the L-heme is potentially five-coordinate (5C), although 5C ferric hemes generally show axial or just slightly rhombic EPR spectra. The observation of this highly rhombic, high-spin ferric species is therefore puzzling, and the nature of the species that gives rise to this EPR signal is not clear. As shown below, the presence of this species is a key difference between the *Ne*CcP and *So*CcP mutants. Upon reduction, the H-heme is reduced into the ferrous state, as evident from the disappearance of the g = 3.40 signal, whereas there is slight change for the L-heme – both the low-spin and the highly rhombic high-spin signals remain in roughly the same intensity ratio.

Resonance Raman Spectra of *Ne*CcP

In resonance Raman (rRaman) spectroscopy, excitation of allowed electronic transitions leads to enhancement of vibrational modes that are coupled to that excitation, either via excited state displacements (**A**-term enhancement) or vibronic coupling (**B**- and **C**-term enhancement).[35] Heme proteins are typically excited with laser wavelengths that correspond to the intense Soret band of the heme or the less intense Q band features at lower energy.[36–37] The bCcP enzymes studied here exhibit ferric Soret bands in the 405–408 nm region and ferrous Soret bands in the 415–417 nm range, and therefore, the 413.1 nm line of a Kr gas ion laser was used here for rRaman studies. Excitation of the Soret band mostly enhances totally symmetric (polarized) vibrations according to the **A**-term mechanism, whereas excitation in the Q band region enhances non-totally symmetric (depolarized) and some anomalously polarized modes (via the **B**- and **C**-term mechanism).[38] In this work, excitation of the samples at 413.1 nm leads to the observation of mostly polarized bands in

the resonance Raman spectra, although some depolarized bands can also be observed. In previous work, the rRaman spectra of many simple heme proteins, including Cyt. *c*[39] and myoglobin,[37, 40] have been analyzed in detail and the different vibrational bands have been assigned and labeled using the υ_n notation, which was first introduced by Kitagawa and coworkers.[41] Importantly, work by Kitagawa, Spiro and others has shown that certain porphyrin core vibrations are sensitive to the oxidation and spin state of the heme,[42–43] and can therefore be used to characterize intermediates in heme proteins.[44]

Figure 4 shows the rRaman spectrum of diferric *Ne*CcP. The single, intense "oxidation state marker band" ν_4 is observed at 1364 cm^{-1} and confirms that the enzyme is indeed in the diferric state. The "spin state marker band" ν_3 (which is actually sensitive to both the oxidation and spin state of the heme) is present at 1504 cm^{-1} and indicates that at least one heme is in the ferric low-spin state. Another spin state sensitive band, ν_2, is observed at 1586 cm^{-1}, which further supports the idea that the hemes are low-spin.[40] The presence of a 5C high-spin ferric heme should manifest itself by the appearance of a ν_3 feature at ~1480 cm^{-1}, which is not observed. Bands at 1547 and 1614 cm^{-1} (ν_{11} and ν_{12}, in this case) suggest that there may be some high-spin ferric heme present in the sample (in agreement with the EPR results). Similarly, the weak ν_3 signal at ~1494 cm^{-1} (a small shoulder on the 1504 cm^{-1} peak) could originate from a six-coordinate (6C) high-spin ferric heme. However, it should be noted that although the bands at 1547 and 1614 cm^{-1} are present in high-spin metMb,[37] they also overlap with features that would be observed for a ferrous heme.[42, 45] Similarly, the ν_3 band at ~1494 cm^{-1} could also correspond to a low-spin ferrous heme. In this regard, a closer inspection of Figure 4b shows a weak signal at 1472 cm^{-1} as well. We conclude that the pair of ν_3 bands at 1472 cm^{-1} (high-spin) and 1494 cm^{-1} (low-spin) most likely corresponds to ferrous heme, which originates from the photoreduction of the H-heme in the presence of the laser light (which is therefore an artifact of the experiment). Note that low-spin ferric Mb also shows a weak signal around 1472 cm^{-1} in the rRaman spectrum, indicating that some of the intensity of this feature might be due to another, unrelated vibration of a low-spin ferric heme.[46] Based on all of these considerations, we therefore conclude that in diferric *Ne*CcP both hemes are mostly in the low-spin ferric state, and that small amounts of ferrous H-heme (due to photoreduction) and potentially a small amount of 6C high-spin ferric L-heme could be present. The data do not, however, support the paradigm that in the constitutively active *Ne*CcP, the L-heme is dominantly in the 5C high-spin ferric state.

Upon one-electron reduction (to the semi-reduced state), the ν_4 oxidation state marker band at 1351 cm^{-1} appears, indicating that the H-heme has now been reduced (Figures 4 and 5). In addition, a decrease of the low-spin ferric marker band ν_3 at 1504 cm^{-1} is observed (which has become a shoulder on the intense 1491 cm^{-1} peak), concomitant with an increase in intensity for the ν_3 bands at 1472 cm^{-1} and 1491 cm^{-1}. These signals are attributed to high-spin and low-spin ferrous heme, respectively, again indicating H-heme reduction and suggesting that this heme can exist in a mixture of spin states (see below).[42] Some of the intensity in the ~1490 cm^{-1} region could also originate from the presence of 6C high-spin ferric L-heme, as discussed above. Importantly, no ν_3 band around 1480 cm^{-1} is observed, again indicating that the ferric L-heme is not in a 5C high-spin state. The ν_2 marker band for a low-spin heme at 1586 cm^{-1} decreases in intensity upon reduction, in agreement with the

idea that some of the reduced (ferrous) heme is actually in the high-spin state. The band at 1560–1563 cm^{-1} is present in both the diferric and the semi-reduced sample, though this band is not as easily assigned. The ν_2 band for a high-spin heme and the ν_{11} band for a ferric heme overlap at 1560–1565 cm^{-1} if both species are present in a single sample.[42] Bands at 1547 and 1614 cm^{-1} are still present in the spectrum, and these bands could result from either a high-spin ferric or a ferrous heme species.[39, 42, 45] The low-spin ferric ν_{10} band at 1640 cm^{-1} has almost entirely disappeared, which suggests that some 6C high-spin ferric heme could be present (in agreement with the EPR data). Based on these results, it appears that in the semi-reduced form of *Ne*CcP, the ferrous H-heme is now in a mixed high-spin/low-spin state, whereas the L-heme is mostly low-spin ferric with potentially a small fraction of 6C high-spin ferric heme present, as in the diferric enzyme. One potential issue with the EPR and rRaman experiments is the fact that they were conducted at cryogenic temperatures, which leaves us with the possibility (playing devil's advocate) that the spin state of the L-heme could be temperature dependent. To help address this issue, resonance Raman data were further collected at room temperature (see below).

Figure 6 shows the rRaman spectrum of the diferric variant *Ne*H59G CcP. There are three ν_4 bands at 1355, 1364, and 1374 cm^{-1}, though the band at 1355 cm^{-1} is power dependent and is therefore due to photoreduction of the H-heme during data collection (Figure S3). Compared to wt enzyme, the spectrum of the H59G mutant shows enhanced photoreduction of the H-heme. From 1400 cm^{-1} to 1700 cm^{-1}, the *Ne*H59G CcP diferric spectrum is quite similar to the spectrum of wild-type *Ne*CcP. The ferric low-spin marker band at 1505 cm^{-1} is more intense in the mutant, and the complete absence of a signal around 1480 cm^{-1} indicates the absence of any 5C high-spin ferric heme. Also, the ν_3 band at 1472 cm^{-1} is now very pronounced, due to the increased photoreduction of the H-heme in the mutant, whereas only a small shoulder appears around 1490 cm^{-1}. This indicates that the photoreduced H-heme is predominantly in the high-spin state, and presumably five-coordinate (due to photochemical cleavage of the Fe-S_{Met} bond upon laser irradiation). The ν_2 spin state marker band for a low-spin heme is present at 1590 cm^{-1}, though this band is broad, and may overlap with another band at slightly higher energy. Potential high-spin ferric bands are present at 1548 and 1614 cm^{-1}, potentially indicating the presence of a small amount of high-spin ferric heme (in agreement with the EPR results). Because these features are not power-dependent like the 1355 cm^{-1} band, they should not be associated with the photoreduced, ferrous heme. Compared to the EPR data, the rRaman spectra do not indicate the presence of an unusual heme, and the highly rhombic, high-spin ferric signal observed by EPR might therefore originate from some other species. Alternatively, if this EPR signal corresponds to a strongly distorted, high-spin heme, this species might only exist at lq. He temperatures and might become low-spin at higher temperatures.

Reduction of the H-heme in the *Ne*H59G CcP mutant results in the disappearance of the ν_4 band at 1374 cm^{-1} (compare Figures 6b and 7b), directly indicating that this feature is associated with the H-heme. Interestingly, in wild-type enzyme the H-heme shows the ν_4 band at 1364 cm^{-1}, which emphasizes that the two hemes in *Ne*CcP influence each other (since the H59G mutation affects the axial ligation of the L-heme). The rRaman spectrum of semi-reduced *Ne*H59G CcP resembles that of semi-reduced wild-type enzyme (compare Figures 5 and 7). Two ν_4 bands are present at 1353 (reduced H-heme) and 1362 cm^{-1} (ferric

L-heme). Three different ν_3 bands are present at 1472, 1494, and 1503 cm^{-1} which can be attributed to high-spin and low-spin ferrous H-heme, and the low-spin ferric L-heme, respectively. Again, no signal is observed at ~1480 cm^{-1} that would be indicative of a 5C high-spin ferric heme. A ν_2 spin-state marker band is present at 1586 cm^{-1}, which indicates the presence of low-spin heme. Bands at 1548 and 1614 cm^{-1} remain, though once again these bands are difficult to immediately assign. Finally, it appears that the low-spin ferric ν_{11} band at 1640 cm^{-1} in the diferric sample has decreased significantly in intensity upon H-heme reduction, indicating less low-spin ferric heme in the sample.

Resonance Raman data were also collected at room temperature for *Ne*CcP and *Ne*H59G CcP (Figures S4 and S5). The room temperature diferric spectra exhibit only one, broad ν_4 band at 1368 cm^{-1} for the wild-type enzyme and at 1360 cm^{-1} for *Ne*H59G CcP. This indicates that photoreduction of the H-heme is suppressed in solution at room temperature, as no ν_4 band around 1355 cm^{-1} is present in the spectra, rendering this an artifact in the low-temperature experiments in a frozen matrix. In addition, there is no band present at 1472 cm^{-1} in the room temperature *Ne*CcP and *Ne*H59G CcP spectra (in contrast to the 77K spectra), in agreement with this. This result further indicates that the 1472 cm^{-1} band in the low-temperature data indeed belongs to the photoreduced, ferrous H-heme. Low-spin ferric marker bands are present in the room temperature spectra for both enzymes at 1500–1502 cm^{-1} and 1636–1637 cm^{-1}. The broad low-spin state marker band ν_2 is present at 1583–1584 cm^{-1} for both samples and bands at 1543–1545 cm^{-1} and 1608 cm^{-1} also appear. These bands could have resulted from the presence of a small amount of ferrous heme in the sample for the low-temperature spectra, but since only one oxidation state marker band appears in each room-temperature spectrum, these bands must then originate from the presence of a different species in solution, likely a small amount of high-spin ferric heme, as indicated by the small, corresponding signal in the EPR data. The absence of any corresponding ν_3 band around 1480 cm^{-1} confirms the absence of 5C high-spin ferric heme in the sample. However, the broad ν_3 band at ~1500 cm^{-1} exhibits a shoulder around 1490 cm^{-1} (especially in wt enzyme), indicating that some 6C high-spin ferric heme could be present.

The room temperature spectra of semi-reduced *Ne*CcP and *Ne*H59G CcP (Figure S5) exhibit a single ν_4 band at 1362 cm^{-1}. Although no ferrous band at 1351 cm^{-1} is visible in the spectrum, this observation likely results from lower spectral resolution as these data were collected at room temperature, which leads to increased band widths. The ν_3 band at 1493 cm^{-1} demonstrates that the reduced H-heme is low-spin at room temperature and that the 1472 cm^{-1} band exclusively observed at low-temperature results from photocleavage of a ligand from the reduced H-heme, resulting in a 5C high-spin site (which is therefore an artifact). The low-spin ferric ν_3 band at 1505 cm^{-1} is less intense than in the diferric enzyme (due to reduction of the H-heme) but is still present under the 1493 cm^{-1} band in both the wild-type and mutant enzymes. A single, broad ν_2 band at 1589 cm^{-1} also indicates that the L-heme is mostly low-spin. As stated above, the bands at 1545 and 1607 cm^{-1} could result from the presence of a small amount of high-spin ferric heme, but these bands are also present in ferrous Cytochrome *c*[39] and thus likely result from the ferrous H-heme. Therefore, our rRaman results demonstrate that in the diferric and semi-reduced states of the wt enzyme at both cryogenic and room temperatures, the L-heme of *Ne*CcP remains largely low-spin.

Magnetic Circular Dichroism of *Ne*CcP

Near UV-visible MCD spectra were recorded at lq. He temperatures for the *Ne*CcP enzyme in both the diferric and semi-reduced states (see Figure 8). The diferric enzyme exhibits a typical MCD spectrum for low-spin ferric hemes with a positive signal at 25130 cm^{-1} and a negative signal at 24050 cm^{-1} in the Soret band region as evident from Figure 8a. In addition, there are low-spin ferric signals in the Q-band region at 20800, 19000, 18490, and 17860 cm^{-1} (see Figure 8b). Upon reduction, the low-spin ferric signals in the Soret region, now at 25280 cm^{-1} and 24300 cm^{-1}, persist, which agrees with the idea that only one of the hemes is reduced. The observation that the ferric L-heme is low-spin is in agreement with the EPR and rRaman data as well. The small, sharp signals at 19720, 19380, 19120, 18720, 18550 and 18160 cm^{-1} that appear upon reduction of the H-heme (Figure 8b) are markers for a diamagnetic (here low-spin ferrous) heme, and they are similar to the MCD signals observed for low-spin ferrous Cyt. c as shown in Figure 2c. The large positive signal at 22860 cm^{-1}, on the other hand, originates from a fraction of the reduced H-heme that is in the high-spin state. In previous studies on *Pa*CcP, it was shown by Foote and co-workers that this signal results from the partial photolysis of the Fe-S_{Met} bond of the reduced H-heme upon irradiation of the sample in the CD spectrophotometer.[16] We further investigated this issue in our own MCD experiments as shown in Figure 9. Here, the signal at 22860 cm^{-1} increases upon photolysis of the sample with a mercury lamp at 2 K, while at the same time the low-spin ferrous signal at 18160 cm^{-1} decreases. This spectral change is reversed upon warming the sample to 70 K in the dark and then cooling the sample back to 2 K, with the low-spin ferrous signal reappearing. Compared to a ferrous Cyt. *c* standard, the low-spin ferrous signal in Figure 8 represents ~62% of the H-heme, and thus the high-spin signal must correspond to the remaining ~38% of the H-heme in this sample. The observed mixture of high-spin and low-spin ferrous H-heme in the semi-reduced sample is directly supported by the rRaman data (see above). There is also a signal at 17,280 cm^{-1} which originates from the high-spin ferrous H-heme. The MCD spectra of diferric and semi-reduced *Ne*H59G CcP are quite similar to wild-type *Ne*CcP (Figure S6). The diferric *Ne*H59G CcP exhibits signals at 24970 and 24030 cm^{-1} in the Soret band region and at 22030, 20650, 18420, and 17140 cm^{-1} in the Q-band region. The semi-reduced spectrum of *Ne*H59G CcP exhibits signals at 25300 and 24320 cm^{-1} in the Soret band region and sharp diamagnetic signals at 19740, 19410, 19150, 18760, 18570 and 18130 cm^{-1} in the Q-band region.

EPR Spectra of *So*CcP (reductively activated)

EPR spectra for both the wild-type *So*CcP and the H80G mutant of the enzyme (*So*H80G CcP) were taken at 12 K. Diferric *So*CcP exhibits an anisotropic low-spin signal at g = 3.38 that disappears upon reduction (Figures 10a and b; a small residual signal is present in the semi-reduced data). This signal results from the "large-g_{max}" H-heme (as observed for *Ne*CcP as well) which is reduced to the ferrous state in the presence of ascorbate.[13] The L-heme shows a strong low-spin signal at 12 K with g = 3.15, and 2.21 in the diferric enzyme. The origin of the weak signal at g = 5.66 is not clear; it could presumably belong to a small amount of high-spin ferric L-heme, although the resonance position would be a bit unusual in this case. Alternatively, this could be due to an impurity. Curiously, in the semi-reduced sample the L-heme now exhibits strong signals at g = 2.89, 2.42, and 1.52 (the remaining, weak signals at 3.15 and 2.21 are due to the incomplete reduction of the H-heme). The latter

resonance positions are similar to those of the L-heme in *Ne*CcP (both diferric and semi-reduced), which indicates that the H-heme influences the properties of the L-heme in ways in *So*CcP that are not observed in *Ne*CcP. More specifically, the L-heme exists in a different state in diferric *So*CcP, likely the bis-His complex, and adopts the same properties as the L-heme in constitutively active *Ne*CcP only after reduction, where the L-Heme is now coordinated by another amino acid side chain or potentially a water/hydroxide molecule (or a mixture of these two possibilities), resulting in a low-spin complex. The EPR spectrum of semi-reduced *So*CcP at pH = 5.5 (shown in Figure S15) is similar to the spectrum at pH = 7, but exhibits a more intense high-spin signal at g ~ 6. This indicates that the low-spin L-heme at pH = 7 is mostly hydroxide-bound and converts to a mixture of high-spin water-bound heme and low-spin hydroxide-bound heme at pH = 5.5. Also, it should be noted here that the conversion from one low-spin L-heme species into a mixture of species upon reduction of the H-heme has previously been reported for *So*CcP.[13]

The EPR spectra of the diferric mutant *So*H80G CcP exhibit similar signals for the H-heme at g = 3.40 and for the L-heme at g = 3.15, 2.21 (low-spin heme) compared to wt. The somewhat mysterious signal at g = 5.66 is also present in the spectrum of the diferric mutant, with an increased intensity. It should be noted here that the *So*CcP “L1-loop” actually contains a pair of His residues, H80 and H81. This observation is singular; no other bCcP has two His residues back to back in the active site. We propose that in *So*H80G CcP, H81 is able to bind to the heme in diferric enzyme, giving rise to similar EPR features for the L-heme compared to wt. Upon reduction, the g = 3.40 signal disappears completely, indicative of complete reduction of the H-heme, but the signals of the L-heme remain at g = 3.10, 2.28 (Figures 10c and d), indicating that H81 remains bound to the heme. The shift of the L-heme resonances upon reduction are therefore only observed for wt enzyme, but not for the mutant, indicating that the mutation of H80 must influence the way that the two hemes communicate. These results are in agreement with previous findings that the H80G mutant is unable to activate upon reduction, resulting in enzyme that shows very little catalytic activity. In semi-reduced *So*H80G CcP, a very small amount of a high-spin ferric heme is also observed, with a signal at g = 5.91. Finally, it is again noteworthy that mutation (removal) of the distal His in *So*H80G CcP does not lead to the formation of a 5C high-spin ferric L-heme, as in the case of the corresponding *Ne*CcP variant. In contrast to *Ne*CcP, the His mutant of *So*CcP does not give rise to the unusual, highly rhombic high-spin signal. As mentioned above, the origin of this signal remains mysterious, since 5C high-spin ferric hemes usually show quite axial EPR signals. This point requires further study.

Resonance Raman Spectra of *So*CcP

In the rRaman spectrum of diferric *So*CcP, shown in Figure 11, the ν_4 oxidation state marker band is observed as a single peak at 1378 cm^{-1}, which confirms that the enzyme is in the diferric state. Curiously, this band is shifted ~14 cm^{-1} to higher energy compared to diferric *NeCcP*. Other marker bands indicative of low-spin ferric heme, ν_3 and ν_{10}, are present at 1508 and 1640 cm^{-1}, respectively. The ν_2 band at 1589 cm^{-1} is analogous to the spin-state marker band for a low-spin heme observed at 1586 cm^{-1} and 1596 cm^{-1} for the diferric *Ne*CcP sample. Interestingly, the *Ne*CcP sample shows two features for ν_2, whereas only a single band is observed for *So*CcP. This indicates that in *Ne*CcP, the two hemes are more

distinct with slightly different vibrational properties compared to *So*CcP. A weak signal is also observed at 1473 cm^{-1}, which might correspond to a small amount of photoreduction of the H-heme as discussed above. Alternatively, this peak could correspond to a different (unrelated) vibrational feature, as no accompanying (low-spin) ferrous ν_4 band is present in the spectrum of diferric *So*CcP. As mentioned above, a corresponding feature is present in low-spin ferric Mb (see discussion for diferric *Ne*CcP).[46] Note that there are no signals present in the spectrum of diferric *So*CcP that correspond to the potential high-spin signals observed at 1547 and 1614 cm^{-1} for diferric *NeCcP*, ruling out the presence of any measurable amounts of a high-spin ferric species in the *So*CcP sample.

Upon reduction of *So*CcP to the semi-reduced state, two new ν_4 bands appear at 1355 and 1363 cm^{-1}, indicating the reduction of the H-heme to the ferrous state (Figure 12; the residual band at 1378 cm^{-1} is likely due to incomplete reduction – see EPR results, or a very small amount of the L-heme that did not convert – see next). Interestingly, for the L-heme, a shift of the ν_4 band from 1378 (diferric) to 1363 cm^{-1} (semi-reduced) is observed, which is further reflected by the change in the EPR parameters of the L-heme: here, the signals shift from g = 3.15, 2.21 (diferric) to g = 2.89, 2.42, 1.52 (semi-reduced). This indicates that the EPR properties of the L-heme and the energy of ν_4 are potentially correlated. Correspondingly, in *Ne*CcP, ν_4 for the L-heme is observed at 1364/1361 cm^{-1} with EPR parameters of g = ~2.9, 2.41, ~1.5, which is fully consistent with these ideas. In the semi-reduced state of *So*CcP, the important spin state marker band ν_3 is observed at 1472 cm^{-1}, indicating the presence of a high-spin ferrous H-heme (in the 5C state, due to photochemical cleavage of the Fe-S_{Met} bond upon laser irradiation). At the same time, the intensity of the low-spin ferric ν_3 band at 1506 cm^{-1} decreases but is still present in the semi-reduced form of the enzyme, in agreement with the idea that one heme remains ferric. However, this feature becomes asymmetric upon reduction, with a shoulder present around ~1490 cm^{-1}. We believe that this shoulder corresponds to the ν_3 band of a small amount of the H-heme that is in the low-spin ferrous state. New bands at 1542 and 1612 cm^{-1} appear in the semi-reduced form which likely result from the ferrous H-heme. These signals could also be evidence for the presence of a small amount of a high-spin ferric heme species at 77 K. Nevertheless, the complete absence of any ν_3 band around 1480 cm^{-1} suggests that no 5C high-spin ferric heme is present in the sample (see discussion for semi-reduced *Ne*CcP above). At the same time, the ν_{10} marker band for a low-spin ferric heme at 1642 cm^{-1} decreases in intensity upon reduction, but does not disappear, again indicating that the L-heme remains largely low-spin ferric in the semi-reduced form of *So*CcP. This leaves us with the contradiction that based on the mechanistic paradigm for reductively activated CcPs, the semi-reduced form should exhibit a 5C, high-spin ferric heme, whereas experimentally, there is no evidence for such a claim. Again, one possible factor that could play a role here is temperature, and correspondingly, the room temperature rRaman data of *So*CcP were also analyzed (see below).

Figure S9 shows the rRaman spectrum of diferric *So*H80G CcP. The spectrum is almost identical to that of wild-type *So*CcP with a ferric ν_4 band present at 1378 cm^{-1}, and two low-spin ferric bands at 1506 and 1640 cm^{-1} (ν_3 and ν_{10} respectively). The low-spin ν_3 band at 1589 cm^{-1} is also observed, as well as a ferric ν_{11} band at 1567 cm^{-1}. These results agree with the EPR results that show that despite the removal of the distal ligand H80 from

the L-heme, this heme remains low-spin in the ferric state with no indication for the presence of a high-spin ferric heme in the rRaman data. Reduction of the H-heme in *So*H80G CcP results in a spectrum that is also similar to the semi-reduced wt *So*CcP data (Figure S10). Two new ν_4 bands are present at 1352 and 1360 cm^{-1} (the residual signal at 1374 cm^{-1} is likely due to incomplete reduction, or incomplete conversion of the L-heme in the reduced form), indicating reduction of the H-heme, as in wild-type *So*CcP. Here, the possible correlation between the ν_3 energy and the EPR resonances of the low-spin L-heme is not fulfilled; the reason for this is not clear. Two easily visible ν_3 bands are present at 1472 and 1501 cm^{-1} which can be attributed to a high-spin ferrous (H-heme) and a low-spin ferric (L-heme) signal, respectively. The 1501 cm^{-1} band is fairly broad and likely conceals a low-spin ferrous ν_3 band ~1490 cm^{-1}, in agreement with the finding for wild-type enzyme that some of the ferrous heme might be in the low-spin state. A ν_2 spin-state marker band is present at 1593 cm^{-1} and indicates the presence of low-spin heme. Two ν_{11} bands are present at 1543 and 1557 cm^{-1}, likely indicating the presence of ferrous and ferric heme in the sample. A ν_{10} band is still present at 1630 cm^{-1}, which is shifted compared to the other low-spin ferric ν_{10} bands for the various CcP samples. The implication of this result is not yet clear. The more pronounced 1608 cm^{-1} band in the diferric sample may result from either ferrous or a high-spin ferric heme species, as in the other samples with signals in the 1608–1614 cm^{-1} range. However, the absence of a ν_3 band around 1480 cm^{-1} again indicates that no 5C high-spin ferric L-heme is present. Our data indicate that most, if not all, of the L-heme is in fact in the low-spin state, as in the case of wt enzyme.

Room temperature rRaman data were also collected for diferric *So*CcP and *So*H59G CcP (Figure S11). Both spectra are very similar to the resonance Raman data taken at 77 K for these enzymes. Only one ν_4 band is present at 1374–1375 cm^{-1}. Bands at 1503–1505 cm^{-1} (ν_3), 1563–1564 cm^{-1} (ν_{11}), and 1638–1640 cm^{-1} (ν_{10}) indicate that in both diferric *So*CcP variants the H- and L-hemes are in the low-spin ferric state. Both spectra exhibit a weak band at 1467–1468 cm^{-1}, which could originate from a small amount of photoreduction of the H-heme, but since no corresponding ν_4 bands are observed at ~1350 cm^{-1}, it is more likely that these small bands are due to other, unrelated vibrations as discussed above (and as observed for low-spin ferric Mb). Room temperature spectra of semi-reduced *So*CcP and *So*H80G CcP are shown in Figure S12. Once again, the ferrous and ferric ν_4 bands were not resolved. Nevertheless, both spectra exhibit ν_3 bands at 1497 and 1504–1509 cm^{-1} indicating the presence of both low-spin ferrous and low-spin ferric hemes. The fact that very small intensity is observed around 1472 cm^{-1} indicates that photochemical cleavage of the Fe-S_{Met} bond of the reduced H-heme is suppressed at room temperature (in contrast to the 77 K data). A single ν_2 spin state band in the 1587–1593 cm^{-1} region also indicates that both hemes are mainly in the low-spin state at room temperature for both the wt enzyme and the variant. The ν_{10} bands in the 1633–1639 cm^{-1} region are also indicative of low-spin ferric heme. So whereas some of the intensity of the 1497 cm^{-1} feature could in principle originate from a 6C high-spin ferric L-heme, other spin state marker bands do not support this possibility. In addition, no evidence for a 5C high-spin ferric L-heme is present in the room temperature rRaman spectra for *So*CcP or *So*H80G CcP.

Magnetic Circular Dichroism Spectra of *So*CcP

Near-UV/visible MCD spectra at lq. He temperatures were recorded for the *So*CcP enzyme in both the diferric and the semi-reduced states (Figure 13). The diferric enzyme exhibits a typical MCD spectrum for low-spin ferric hemes with a positive signal at 25000 cm^{-1} and a negative signal at 24300 cm^{-1} in the Soret band region. In addition, there are low-spin ferric signals present in the Q-band region at 20870, 19050, 18510, and 17980 cm^{-1}. This spectrum exhibits very similar features compared to the MCD spectrum of diferric *Ne*CcP (Figure 8). Both of these peroxidases seem to possess low-spin ferric hemes at lq. He temperature. Upon reduction, the low-spin ferric signals at 25280 cm^{-1} and 24310 cm^{-1} are still present, though they have decreased in intensity significantly, in agreement with the idea that one of the hemes has become reduced. The large positive signal at 22880 cm^{-1} results from the reduced H-heme in the high-spin state. As described before in the literature (for *Pa*CcP)[16] and observed for *Ne*CcP (Figure 8), this signal results from the partial photolysis of the Fe-S_{Met} bond in the H-heme upon irradiation of the sample in the CD spectrophotometer. The H-heme continues to undergo photolysis over time, though some low-spin ferrous heme remains, which is evident from the sharp diamagnetic signals in the Q-band region of the semi-reduced form at ~18160 cm^{-1}. Compared to a ferrous Cyt. *c* standard, the low-spin ferrous signal represents ~32% of the H-heme in the data shown in Figure 13b, and thus, the high-spin signal results from the remaining ~68% of the ferrous heme in this sample. Photolysis can be reversed by warming the sample to 70 K in the dark and then cooling the sample back down to 2 K (Figure 14), which also works for *Ne*CcP (Figure 9). Both diferric and semi-reduced *So*H80G CcP samples exhibit similar signals compared to wild-type *So*CcP. The spectrum of diferric *So*H80G CcP exhibits signals at 25010 and 24280 cm^{-1} in the Soret band region and at 22330, 20820, 18490, and 17160 cm^{-1} in the Q-band region (Figure S13). The spectrum of semi-reduced *So*H80G CcP exhibits signals at 25080 and 24290 cm^{-1} in the Soret band region and sharp diamagnetic signals at 19720, 19380, 19130, and 18090 cm^{-1} in the Q-band region. A high-spin ferrous heme signal is present at 22850 cm^{-1} due to some photolysis of the sample.

Discussion

In this study, EPR, resonance Raman, and MCD spectra were collected in order to elucidate the differences between the ‘constitutively active’ bCcP from *Nitrosomonas europaea* (*Ne*CcP) and the ‘reductively activated’ bCcP from *Shewanella oneidensis* (*So*CcP). Prior work on the reactivity and crystallographic structure of the constituitively active *Ne* enzyme indicate that the L-heme is five-coordinate (5C) and (presumably) high-spin. [3, 19] In contrast, studies of the activatable enzymes suggest that reduction of the His/Met-ligated H-heme is required for the L-heme to become 5C (no water or exogenous ligand bound).[2, 7] We turned to a side-by-side approach comparing the *Ne* and *So* enzymes as relevant systems for those bCcPs that are constituitively active and those that require reductive activation. Key spectroscopic results and assignments for the H-heme and L-heme in *Ne*CcP are summarized in Table 1.

Diferric *NeCcP* Spectroscopy.

Starting with the resting state (diferric) of the recombinant *Ne*CcP, EPR data assigned to both the H-heme (g = 3.41) and the L-heme (g = 2.91, 2.41, and 1.50) indicate low-spin states (at 12 K), and hence, six-coordinate (6K) coordination environments. A small amount of high-spin ferric species is also present at g = 6.15, but this is only a very small percentage of the sample. This result is similar to previous EPR investigations on the natively expressed *Ne*CcP that show one low-spin signal for the H-heme, and a major low-spin component and a small high-spin signal for the L-heme.[3] Our additional spectroscopic characterization bear this out. For example, the low-temperature MCD spectrum of diferric *Ne*CcP shows only signals originating from low-spin ferric hemes (since MCD signals from low-spin and high-spin ferric hemes sometimes overlap, and the signals from the low-spin form are much more intense,[16] the MCD results are less conclusive in ruling out a 5C high-spin form for the L-heme compared to the EPR data). Under cryogenic conditions, it is clear that both the H-heme and the L-heme in diferric *Ne*CcP are low-spin, and correspondingly 6C. Previous studies on the activatable *Pa*CcP have shown that the spin state of the L-heme is temperature-dependent,[16–17] and at He temperatures, the L-heme is mostly or completely low-spin. To further investigate this point, we followed these experiments with rRaman studies on diferric *Ne*CcP at 77 K, where the potential spin state change should not be an issue. In the rRaman data, a single ν_4 oxidation state marker band is visible at 1364 cm^{-1}, and a single ν_3 spin state marker band is observed at 1504 cm^{-1}, indicative of predominant low-spin ferric heme in the sample. This is further confirmed by the absence of a ν_3 signal at ~1480 cm^{-1}, which is a hallmark of 5C high-spin ferric heme.[37] Again, only small traces of high-spin signals could be observed: small signals at 1547 and 1614 cm^{-1}, previously assigned as ν_{11} and ν_{10} for high-spin ferric myoglobin, could also result from a small amount of photoreduction.[37] In addition, a 6C high-spin form could contribute to the signal at 1494 cm^{-1}. To further eliminate the possibility of a cryogenic affect, room temperature rRaman data were collected as well, but failed to detect any significant amounts of a 5C high-spin ferric heme species. In summary, our spectroscopic results obtained at 12 K, 77 K, and at room temperature do not support the previously proposed paradigm that the L-heme in diferric *Ne*CcP is predominantly 5C, and hence, high-spin.

Given the surprising nature of these results, we turned to a mutagenesis strategy, examining the *Ne*H59G variant, which is devoid of the conserved His residue found in the activatable bCcP family members. The EPR data of diferric *Ne*H59G CcP indicate that the L-heme exists in the low-spin state (g = 2.90, 2.41, 1.57), and, in addition, a very unusual, highly rhombic high-spin signal (g = 4.82, 4.09, and 3.78) is also present in the data. The origin of this signal is not clear. Only an extremely small $g \sim 6$ high-spin ferric heme signal is observed in the sample. It is striking that the EPR resonances observed for the L-heme are identical for wt enzyme and the mutant, which provides strong evidence that the L-heme does not actually correspond to a bis-His site, but actually has a different distal ligand, either another amino acid side chain and/or water/hydroxide, to result in a low-spin state. As there are no other obvious ligands, the presence of a bound hydroxide seems most likely (as a His/water ligated heme is likely high-spin).[47] Resonance Raman data for the *Ne*H59G CcP mutant are similar to wt enzyme: again, there is no evidence for any significant amount of a 5C high-spin ferric heme in the rRaman data. Intriguingly, *Ne*H59G CcP shows an increased

amount of photoreduction of the H-heme compared to wt, and the ν_4 marker band of the H-heme is shifted (to 1374 cm^{-1}) when compared to wt, indicating that mutation localized at one heme can influence the properties of the other.

Comparisons to *So*CcP.

Key spectroscopic results and assignments for the H-heme and L-heme in *So*CcP are summarized in Table 2. The EPR spectra of *So*CcP matches our prior reports,[13] though in the current set of experiments, we no longer purify the *So* enzyme with a cleavable maltose-binding protein tag, as that led to spectroscopic signals post-cleavage that were artifacts. Here we find that the H-heme shows the typical signal at $g = 3.40$ like the *Ne* enzyme, whereas the resonances of the L-heme are different (g = 3.15, 2.21). Just as in the case of *Ne*CcP, there is no evidence for the presence of any significant amount of a 5C high-spin ferric heme in the EPR data, or in the low-temperature MCD data (even with the caveat that the presence of a smaller amount of a high-spin ferric heme species would be less noticeable in the MCD data compared to EPR), or in the rRaman data. In particular: the rRaman spectrum of diferric *So*CcP (77 K), shows one ν_4 ferric oxidation state marker band at 1378 cm^{-1}, a single ν_2 low-spin marker band at 1589 cm^{-1}, and important spin and oxidation state marker bands ν_3 and ν_{11} are observed at 1504 cm^{-1} and 1640 cm^{-1}. All of these are indicators of the presence of low-spin ferric heme. Further, we see no indication for a spin crossover, even in the room temperature rRaman spectrum of *So*CcP. In comparison to *Ne*CcP, we assign the L-heme to the bis-His complex, based on the differences in EPR resonances.

In analogy to *Ne*CcP, we also investigated the equivalent distal His mutant of *So*CcP, SoH80G CcP, to determine whether a five-coordinate, high-spin ferric L-heme could be obtained in this way. Notably, the loop which bears the ligating H80 contains a second His residue (H81), a unique feature of the *So* enzyme that is not found in any other characterized bCcP. The EPR data of diferric H81G are essentially identical to that of wild-type *So*CcP (g values of 3.40 (H-heme) and 3.15, 2.21 (L-heme)). Unlike *Ne*H59G, the highly rhombic high-spin signal was not observed. This suggests that in *So*H80G CcP, the L-heme is able to recruit an additional ligand instead of the native H80, which is likely H81, resulting again in a bis-His complex. With this hypothesis, it is not surprising that the rRaman spectra of *So*H80G CcP at both cryogenic (77 K) and room temperature are very similar to those of wild-type (wt) enzyme and again show the presence of low-spin ferric hemes only, despite the removal of the H80 residue of the L-heme in the mutant. One interesting difference to *Ne*CcP is the fact that no significant photoreduction of the H-heme is observed in the 77 K rRaman data of *So*H80G CcP, whereas in *Ne*CcP and *Ne*H59G CcP the photoreduction of the H-heme is enhanced.

While the lack of observable 5C high-spin L-heme for the *Ne* enzyme was a surprise, its absence was not a surprise for the activatable *So*CcP where reduction of the H-heme is required for the L-heme to become activated. Thus, we turned to the semi-reduced states of *So*CcP and *Ne*CcP enzymes, where we might anticipate finding 5C ferric L-hemes.

Semi-reduced *Ne*CcP and *So*CcP.

In general, the semi-reduction of either *Ne*CcP or *So*CcP is readily achieved with ascorbate, and followed optically, as well as by EPR. The EPR spectra show the specific disappearance of the anisotropic, "large g_{max}," low-spin signal at $g = 3.41$ for *Ne* and 3.38 for the *So* enzyme.[33, 34] For the *Ne* enzyme, the low-spin L-heme signals are unchanged in the semi-reduced form, as is the case for the corresponding low-temperature MCD spectrum; both indicate that the L-heme continues to be in the low-spin state. Changes in the MCD data indicate that the H-heme is reduced: new features are observed at 22860 cm^{-1} and a derivative-shaped, sharp signal occurs at 18160 cm^{-1} (assigned to the Q-band), accompanied by a number of smaller, equally sharp peaks (the vibronic Q_v band). While the sharp features are a hallmark of a diamagnetic, low-spin ferrous heme, the feature at 22860 cm^{-1} corresponds to ferrous heme in the high-spin state, resulting from the photolysis of the Fe-S_{Met} bond of the reduced H-heme.[16] Resonance Raman measurements further corroborate these results: the spectrum of semi-reduced *Ne*CcP exhibits two ν_4 oxidation state marker bands at 1351 and 1361 cm^{-1}, confirming the presence of a ferric and a ferrous heme. The ν_2 band at 1586 cm^{-1} decreases in intensity compared to the diferric form, which indicates a decrease in the concentration of low-spin heme in the sample. The decrease in intensity of ν_3 at 1504 cm^{-1} and ν_{10} at 1640 cm^{-1} is in agreement with this, showing a loss in low-spin ferric heme upon reduction. At the same time, new ν_3 bands at 1472 and 1492 cm^{-1} occur, which confirm the presence of a ferrous heme, both in the high-spin and low-spin heme state (the high-spin state results from photolysis during the rRaman experiment). As in the diferric enzyme, no ν_3 signal is observed at ~1480 cm^{-1}, indicating the absence of any significant amount of a 5C high-spin ferric heme. Small signals at 1544 cm^{-1} and 1611 cm^{-1} persist, which may indicate the presence of a small amount of a 6C high-spin ferric heme, which would then also contribute to the intensity of the 1492 cm^{-1} feature (though similar features are also present in ferrous heme samples).[39, 42] In summary, reduction of the H-heme has no significant effect on the spectroscopic properties of the L-heme in *Ne*CcP, which makes intuitive sense, since in constitutively active bCcPs, reduction of the H-heme is not required for catalysis. Yet, we cannot observe the L-heme as a static, 5C and high-spin entity.

These conclusions also hold for the mutant *Ne*H59G CcP. In the EPR spectrum of *Ne*H59G CcP, the H-heme signal at g = 3.40 disappears upon reduction, but otherwise, no change is observed for the low-spin signal of the L-heme. The unusual, highly rhombic high-spin signal also persists. The rRaman spectrum of semi-reduced *Ne*H59G CcP is very similar to that of wild-type semi-reduced *Ne*CcP, with only slight shifts in the wavenumbers of the relevant bands. No significant amounts of a 5C high-spin ferric heme (which should give rise to a quite axial EPR signal) are observed for semi-reduced *Ne*H59G CcP either.

In contrast, semi-reduction of *So*CcP produces significant changes: while the reduction of the H-heme results in bleaching of the $g = 3.38$ EPR feature, the signals for the L-heme are *also* shifted relative to the diferric enzyme. In diferric *So*CcP, the L-heme resonances are observed at g = 3.15, 2.21, which shift to 2.89, 2.42, 1.52 in the semi-reduced form. The latter resonance positions are almost identical to those of the L-heme in *Ne*CcP (both diferric and semi-reduced, see above), indicating that indeed, reduction of the H-heme

results in changes that make the active site spectroscopically identical to what one finds in the constitutively active enzyme. The appearance of a ferric ν_4 band at 1363 cm^{-1} in the rRaman spectrum of semi-reduced *So*CcP is similar to the corresponding signal in *Ne*CcP (both for the diferric and semi-reduced form) at 1361 cm^{-1} and supports this change in the active site of the *So*CcP L-heme. The activation chemistry indicates a swap of the distal ligand of the L-heme upon reduction of *So*CcP, resulting in an altered 6C complex, but is not associated with converting the L-heme into a static, 5C high-spin ferric heme.

The data thus far suggest that as the distal His is either absent (constitutively active bCcP family members) or lost upon reduction (activatable bCcP enzyme family), it is replaced with an additional, exchangeable ligand, such as hydroxide. Hence, the active form of a bCcP does not involve a 5C high-spin ferric active site. Using the crystal field parameters of Taylor,[48] the *g*-values for both semi-reduced *So*CcP and diferric (and semi-reduced) *Ne*CcP are at 2.89 and 2.42, which corresponds to a site with His/anionic ligand coordination, whereas the g-values of the *So* enzyme (3.15, and 2.21; in agreement with prior reports for other activatable bCcPs[15, 49]), correspond to a bis-imidazole bound heme. In addition, EPR data taken at pH = 5.5 (Figure S15) suggest that semireduced *So*CcP is mostly hydroxide-bound at pH = 7, as the high-spin signal at g ~ 6 increases at lower pH, indicating a conversion between hydroxide and water. Prior structural studies of the *Pa* and *Paracoccus pantotrophus* CcPs further support these ideas, as in both cases a water molecule was modeled into the active site for the semi-reduced enzymes.[8, 15] Thus, we have demonstrated that spectroscopically, a strongly coordinating anionic ligand is bound to bCcPs in their active state, precluding the generation of typical 5C high-spin ferric spectral features (Figure 15). Collectively, these results point towards a subtler activation mechanism of reductively activated bCcPs then previously realized.

Mechanistic Implications.

As described above in detail, our spectroscopic data for diferric and semi-reduced *Ne*CcP and *So*CcP and their mutants implicate that in both types of bCcPs (activatable and constitutively active) the active site heme iron is likely never ‘naked’ and 5C. All our spectroscopic data - EPR, MCD and rRaman, determined at 2K, 12 K, 77 K, and room temperature – only show the presence of small amounts of a high-spin ferric heme, if any at all. In both cases, the L-heme does not exist in a static, 5C high-spin ferric state in the active form of the enzyme (either diferric (*Ne*CcP) or semi-reduced (*So*CcP)), in contrast to what might be found in other heme peroxidases. This conclusion suggests that a more dynamic process is at work in generating an active state that can participate in catalysis, ensuring that 5C heme is not achieved.

On the other hand, our spectroscopic results point to a completely different explanation for the activation process of bCcPs that is much more subtle in so far as reduction of the H-heme can guide specific ligand exchange reactions of the L-heme distal His, and binding of water at the active site, in lieu of the native substrate (Scheme 2). The water molecule would then be deprotonated, generating a low-spin ferric heme with bound hydroxide. In addition, the small amounts of a 6C high-spin ferric heme observed in our spectroscopy could then be explained with the formation of the corresponding water-bound L-heme. Upon entrance of

the substrate hydrogen peroxide into the active site, an acid base reaction could occur where the hydroxide ligand deprotonates the hydrogen peroxide, forming a water molecule that is then easily displaced by the hydroperoxo anion, generating the low-spin heme-hydroperoxo complex in the first step of catalysis. This is followed by formation of Compound I- or Compound Il-like intermediates, and ultimately generation of water. Future work will focus on gathering further evidence for this new mechanism of activation for bCcPs.

Most importantly, these mechanistic possibilities help distinguish canonical bCcP enzymes from MauG, a bCcP superfamily member where formation of a 5C heme in the active state of the enzyme has been established by EPR and rRaman spectroscopy.[23–24] MauG catalyzes the oxidation and oxygenation of two tryptophan residues to TTQ in the protein methylamine dehydrogenase (MADH). The activity of MauG must be induced after binding to MADH, and therefore, a five-coordinate peroxidatic heme may be required to efficiently bind H_2O_2/O_2 to form an Fe^{IV}=O unit in the MauG/MADH complex. Whether or not the relationship is causal or coincidental, the appearance of a true 5C heme appears to be important for the generation of the highly oxidizing intermediates that would be required to install the TTQ cross-link, but which are not required of a cytochrome *c* oxidizing bCcP that scavenges H_2O_2 as its primary function. The activity of bCcPs is dependent on peroxide concentration in the bacterial periplasm and a mechanism that requires H_2O_2 to replace a heme-bound ligand could allow for peroxide binding as H_2O_2 accumulates while also allowing for facile protein ligand re-binding at low H_2O_2 concentration. *Ne*CcP has previously been crystallized at room temperature over two days with the L-heme in the 5C state,[19, 50] though this coordination state may have resulted from dissociation of a water/hydroxide ligand during crystallization. It is evident that dynamic exchange of a sixth (aquo/hydroxo) ligand may help to stabilize the heme site prior to catalysis.

In addition, the redox potential and coordination environment of the H-heme in bCcPs also lie in contrast to MauG as both hemes in MauG exhibit low, and similar redox potentials (−159 and −240 mV).[24] Reduction of the H-heme is required in activatable bCcPs prior to catalysis, though our results indicate that the reduction of the H-heme in *So*CcP does not lead to the formation of a static 5C ferric L-heme, but rather to the formation of a hydroxo complex which in turn may be the key to reducing H_2O_2 to water with high specificity. On the other hand, the peroxidatic heme in MauG likely does not require water binding as the heme exists in a static, 5C high-spin state in the native enzyme. Despite the structural similarities between MauG and bCcPs, the heme spin states and coordination states as further described here are quite different between the two enzymes, leading to unique function and mechanisms.

Supplementary Material

Refer to Web version on PubMed Central for supplementary material.

ACKNOWLEDGMENTS

The authors would like to acknowledge Prof. Hannah Shafaat and Ms. Anastasia Manesis at Ohio State University for their aid in the collection of some of the room temperature rRaman data, and Mr. Bradley Musselman (University of Michigan) for help with collecting some of the EPR data. Financial support for this work from the

University of Michigan, Associate Professor Support Fund (to NL), and the National Institutes of Health (R01-GM110390 to SJE and NL), is gratefully acknowledged. MWW thanks the Rackham Graduate School and the Department of Chemistry (both University of Michigan) for financial support in the form of Graduate Student Fellowships.

REFERENCES

1. Chandel NS; McClintock DS; Feliciano CE; Wood TM; Melendez JA; Rodriguez AM; Schumacker PT (2000) Reactive oxygen species generated at mitochondrial complex III stabilize hypoxia-inducible factor-1alpha during hypoxia: a mechanism of O_2 sensing. J. Biol. Chem 275, 25130–25138. [PubMed: 10833514]
2. Pettigrew GW; Echalier A; Pauleta SR (2006) Structure and mechanism in the bacterial dihaem cytochrome c peroxidases. J. Inorg. Biochem 100, 551–567. [PubMed: 16434100]
3. Arciero DM; Hooper AB (1994) A di-heme cytochrome c peroxidase from Nitrosomonas europaea catalytically active in both the oxidized and half-reduced states. J. Biol. Chem 269, 11878–11886. [PubMed: 8163487]
4. Ellfolk N; Ronnberg M; Aasa R; Andreasson LE; Vanngard T. (1983) Properties and function of the two hemes in Pseudomonas cytochrome c peroxidase. Biochim. Biophys. Acta 743, 23–30. [PubMed: 6297595]
5. Pettigrew GW.; Prazeres S; Costa C; Palma N; Krippahl L; Moura I; Moura JJ (1999) The structure of an electron transfer complex containing a cytochrome c and a peroxidase. J. Biol. Chem 274, 11383–11389. [PubMed: 10196231]
6. Pettigrew GW; Pauleta SR; Goodhew CF; Cooper A; Nutley M; Jumel K; Harding SE; Costa C; Krippahl L; Moura I; Moura J. (2003) Electron transfer complexes of cytochrome c peroxidase from Paracoccus denitrificans containing more than one cytochrome. Biochemistry 42, 11968–11981. [PubMed: 14556628]
7. Ronnberg M; Ellfolk N. (1978) Pseudomonas cytochrome c peroxidase. Initial delay of the peroxidatic reaction. Electron transfer properties. Biochim. Biophys. Acta 504, 60–66. [PubMed: 213111]
8. Echalier A; Goodhew CF; Pettigrew GW; Fulop V. (2006) Activation and catalysis of the di-heme cytochrome c peroxidase from Paracoccus pantotrophus. Structure 14, 107–117. [PubMed: 16407070]
9. Alves T; Besson S; Duarte LC; Pettigrew GW; Girio FM; Devreese B; Vandenberghe I; Van Beeumen J; Fauque G; Moura I. (1999) A cytochrome c peroxidase from Pseudomonas nautica 617 active at high ionic strength: expression, purification and characterization. Biochim. Biophys. Acta 1434, 248–259. [PubMed: 10525144]
10. De Smet L; Pettigrew GW; Van Beeumen JJ (2001) Cloning, overproduction and characterization of cytochrome c peroxidase from the purple phototrophic bacterium Rhodobacter capsulatus. Eur. J. Biochem 268, 6559–6568. [PubMed: 11737210]
11. Timoteo CG; Tavares P; Goodhew CF; Duarte LC; Jumel K; Girio FM; Harding S; Pettigrew GW; Moura I. (2003) Ca^{2+} and the bacterial peroxidases: the cytochrome c peroxidase from Pseudomonas stutzeri. J. Biol. Inorg. Chem 8, 29–37. [PubMed: 12459896]
12. Hoffmann M; Seidel J; Einsle O. (2009) CcpA from Geobacter sulfurreducens is a basic di-heme cytochrome c peroxidase. J. Mol. Biol 393, 951–965. [PubMed: 19735665]
13. Pulcu GS; Frato KE; Gupta R; Hsu HR; Levine GA; Hendrich MP; Elliott SJ (2012) The diheme cytochrome c peroxidase from Shewanella oneidensis requires reductive activation. Biochemistry 51, 974–985. [PubMed: 22239664]
14. Seidel J; Hoffmann M; Ellis KE; Seidel A; Spatzal T; Gerhardt S; Elliott SJ; Einsle O. (2012) MaCA is a Second Cytochrome c Peroxidase of Geobacter. Biochemistry 51, 2747–2756. [PubMed: 22417533]
15. Echalier A; Brittain T; Wright J; Boycheva S; Mortuza GB; Fulop V; Watmough NJ (2008) Redox-linked structural changes associated with the formation of a catalytically competent form of the diheme cytochrome c peroxidase from Pseudomonas aeruginosa. Biochemistry 47, 1947–1956. [PubMed: 18217775]

16. Foote N; Peterson J; Gadsby PM; Greenwood C; Thomson AJ (1985) Redox-linked spin-state changes in the di-haem cytochrome c-551 peroxidase from Pseudomonas aeruginosa. Biochem. J 230, 227–237. [PubMed: 2996492]
17. Foote N; Peterson J; Gadsby PM; Greenwood C; Thomson AJ (1984) A study of the oxidized form of Pseudomonas aeruginosa cytochrome c-551 peroxidase with the use of magnetic circular dichroism. Biochem. J 223, 369–378. [PubMed: 6093773]
18. Zahn JA; Arciero DM; Hooper AB; Coats JR; DiSpirito AA (1997) Cytochrome c peroxidase from Methylococcus capsulatus Bath. Arch. Microbiol 168, 362–372. [PubMed: 9325424]
19. Shimizu H; Schuller DJ; Lanzilotta WN; Sundaramoorthy M; Arciero DM; Hooper AB; Poulos TL (2001) Crystal structure of Nitrosomonas europaea cytochrome c peroxidase and the structural basis for ligand switching in bacterial Di-heme peroxidases. Biochemistry 40, 13483–13490. [PubMed: 11695895]
20. Frato KE; Walsh KA; Elliott SJ (2016) Functionally Distinct Bacterial Cytochrome c Peroxidases Proceed through a Common (Electro)catalytic Intermediate. Biochemistry 55, 125–132. [PubMed: 26575087]
21. Bradley AL; Chobot SE; Arciero DM; Hooper AB; Elliott SJ (2004) A distinctive electrocatalytic response from the cytochrome c peroxidase of Nitrosomonas europaea. J. Biol. Chem 279, 13297–13300. [PubMed: 14973133]
22. Jensen LMR; Sanishvili R; Davidson VL; Wilmot CM (2010) In Crystallo Posttranslational Modification Within a MauG/Pre-Methylamine Dehydrogenase Complex. Science 327, 1392–1394. [PubMed: 20223990]
23. Wang YT; Graichen ME; Liu AM; Pearson AR; Wilmot CM; Davidson VL (2003) MauG, a novel diheme protein required for tryptophan tryptophylquinone biogenesis. Biochemistry 42, 7318–7325. [PubMed: 12809487]
24. Li XH; Feng ML; Wang YT; Tachikawa H; Davidson VL (2006) Evidence for redox cooperativity between c-type hemes of MauG which is likely coupled to oxygen activation during tryptophan tryptophylquinone biosynthesis. Biochemistry 45, 821–828. [PubMed: 16411758]
25. Li XH; Fu R; Lee SY; Krebs C; Davidson VL; Liu AM (2008) A catalytic di-heme bis-Fe(IV) intermediate, alternative to an Fe(IV)=O porphyrin radical. Proc. Natl. Acad. Sci 105, 8597–8600. [PubMed: 18562294]
26. Arslan E; Schulz H; Zufferey R; Kunzler P; Thony-Meyer L. (1998) Overproduction of the Bradyrhizobium japonicum c-type cytochrome subunits of the cbb(3) oxidase in Escherichia coli. Biochem. Biophys. Res. Commun 251, 744–747. [PubMed: 9790980]
27. Paulat F; Lehnert N. (2008) Detailed assignment of the magnetic circular dichroism and UV-vis spectra of five-coordinate high-spin ferric [Fe(TPP)(Cl)]. Inorg. Chem 47, 4963–4976. [PubMed: 18438984]
28. Galinato MGI; Spolitak T; Ballou DP; Lehnert N. (2011) Elucidating the Role of the Proximal Cysteine Hydrogen-Bonding Network in Ferric Cytochrome P450cam and Corresponding Mutants Using Magnetic Circular Dichroism Spectroscopy. Biochemistry 50, 1053–1069. [PubMed: 21158478]
29. Lehnert N. (2012) Elucidating second coordination sphere effects in heme proteins using low-temperature magnetic circular dichroism spectroscopy. J. Inorg. Biochem 110, 83–93. [PubMed: 22516139]
30. Vickery L; Nozawa T; Sauer K. (1976) Magnetic circular dichroism studies of low-spin cytochromes. Temperature dependence and effects of axial coordination on the spectra of cytochrome c and cytochrome bs. J. Am. Chem. Soc 98, 351–357. [PubMed: 1438]
31. Vickery L; Nozawa T; Sauer K. (1976) Magnetic circular dichroism studies of myoglobin complexes. Correlations with heme spin state and axial ligation. J. Am. Chem. Soc 98, 343–350. [PubMed: 173751]
32. Gouterman M; Snyder LC; Wagniere GH (1963) Spectra of Porphyrins: Part II. Four Orbital Model. J. Mol. Spectrosc 11, 108–127.
33. Walker FA (2004) Models of the Bis-Histidine-Ligated Electron-Transferring Cytochromes. Comparative Geometric and Electronic Structure of Low-Spin Ferro- and Femhemes. Chem. Rev 104, 589–615. [PubMed: 14871136]

34. Zoppellaro G; Bren KL; Ensign AA; Harbitz E; Kaur R; Hersleth H-P; Ryde U; Hederstedt L; Andersson KK (2009) Studies of Ferric Heme Proteins with Highly Anisotropic/Highly Axial Low Spin (S=1/2) Electron Paramagnetic Resonance Signals with bis-Histidine and Histidine Methionine Axial Iron Coordination. Biopolymers 91, 1064–1082. [PubMed: 19536822]
35. Spiro TG, R. S. C., Resonance Raman Spectroscopy. In Physical Methods in Bioinorganic Chemistry: Spectroscopy and Magnetism, Que L, Ed. University Science Books: Sausalito, CA, 2010; pp 59–119.
36. Strekas TC; Spiro TG (1974) Resonance-raman evidence for anomalous heme structures in cytochrome c' from Rhodopseudomonas palustris. Biochim. Biophys. Acta 351, 237–245. [PubMed: 4366150]
37. Hu SS,KM; Spiro TG (1996) Assignment of protoheme resonance Raman spectrum by heme labeling in Myoglobin. J. Am. Chem. Soc 118, 12638–12646.
38. Paulat F; Praneeth VK; Nather C; Lehnert N. (2006) Quantum chemistry-based analysis of the vibrational spectra of five-coordinate metalloporphyrins [M(TPP)Cl]. Inorg. Chem 45, 2835–2856. [PubMed: 16562940]
39. Hu SZ; Morris IK; Singh JP; Smith KM; Spiro TG (1993) Complete Assignment of Cytochrome-C Resonance Raman-Spectra Via Enzymatic Reconstitution with Isotopically Labeled Hemes. J. Am. Chem. Soc 115, 12446–12458.
40. Kitagawa T; Kyogoku Y; Iizuka T; Saito MI (1976) Nature of the iron-ligand bond in ferrous low spin hemoproteins studied by resonance Raman scattering. J. Am. Chem. Soc 98, 5169–5173. [PubMed: 182732]
41. Abe M; Kitagawa T; Kyogoku Y. (1978) Resonance Raman-Spectra of Octaethylporphyrinato-Ni(II) and Meso-Deuterated and N-15 Substituted Derivatives .II. A Normal Coordinate Analysis. J. Chem. Phys 69, 4526–4534.
42. Spiro TG; Strekas TC (1974) Resonance Raman-Spectra of Heme Proteins - Effects of Oxidation and Spin State. J. Am. Chem. Soc 96, 338–345. [PubMed: 4361043]
43. Kitagawa T; Ozaki Y; Teraoka J; Kyogoku Y; Yamanaka T. (1977) PH-Dependence of Resonance Raman-Spectra and Structural Alterations at Heme Moieties of Various C-Type Cytochromes. Biochim. Biophys. Acta 494, 100–114. [PubMed: 20152]
44. Ruetz M; Kumutima J; Lewis BE; Filipovic MR; Lehnert N; Stemmler TL; Banerjee R. (2017) A distal ligand mutes the interaction of hydrogen sulfide with human neuroglobin. J. Biol. Chem 292, 6512–6528. [PubMed: 28246171]
45. Uno T; Nishimura Y; Tsuboi M. (1984) Time-Resolved Resonance Raman-Study of Alkaline Isomerization of Ferricytochrome-C. Biochemistry 23, 6802–6808.
46. Bostelaar T; Vitvitsky V; Kumutima J; Lewis BE; Yadav PK; Brunold TC; Filipovic M; Lehnert N; Stemmler TL; Banerjee R. (2016) Hydrogen Sulfide Oxidation by Myoglobin. J. Am. Chem. Soc 138, 8476–8488. [PubMed: 27310035]
47. Varadarajan R; Lambright DG; Boxer SG (1989) Electrostatic interactions in wild-type and mutant recombinant human myoglobins. Biochemistr 28, 3771–3781.
48. Taylor CPS (1977) Epr of Low-Spin Heme Complexes - Relation of T2g Hole Model to Directional Properties of G-Tensor, and a New Method for Calculating Ligand-Field Parameters. Biochim. Biophys. Acta 491, 137–149. [PubMed: 191085]
49. Gilmour R; Goodhew CF; Pettigrew CW; Prazeres S; Moura I; Moura JJ (1993) Spectroscopic characterization of cytochrome c peroxidase from Paracoccus denitrificans. Biochem. J 294, 745–752. [PubMed: 8397509]
50. Pappa H; Li H; Sundaramoorthy M. (1996) Crystallization and Preliminary Crystallographic Analysis of Cytochrome c553 Peroxidase from Nitrosomonas europaea. J. Struc. Biol 116, 429–431.

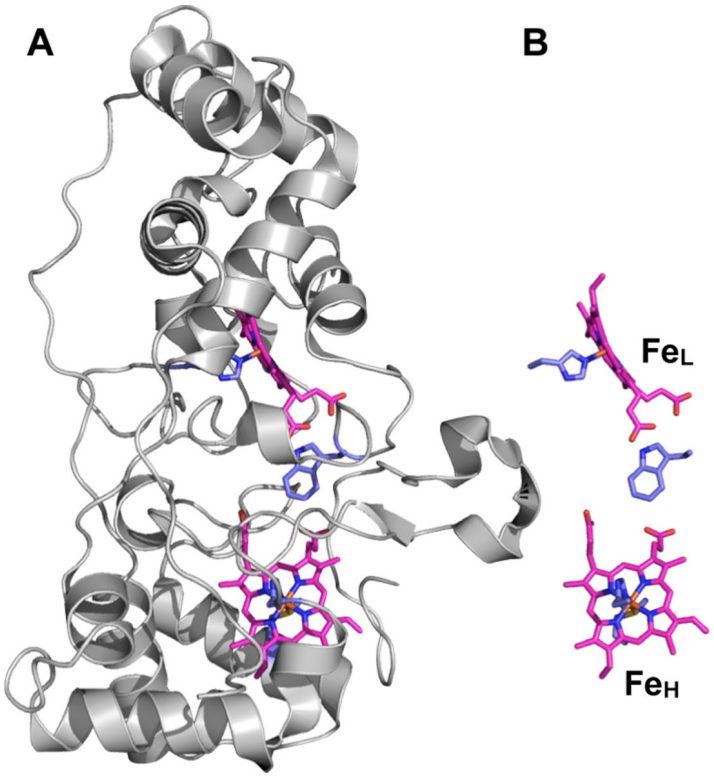

Figure 1.

A) Canonical fold of an constitutively active bCcP family protomer (1IQC.pdb, ref 18), which includes B) a presumed five-coordinate low-potential peroxidatic active site (FeL) and a His-/Met-ligated high potential heme (FeH).

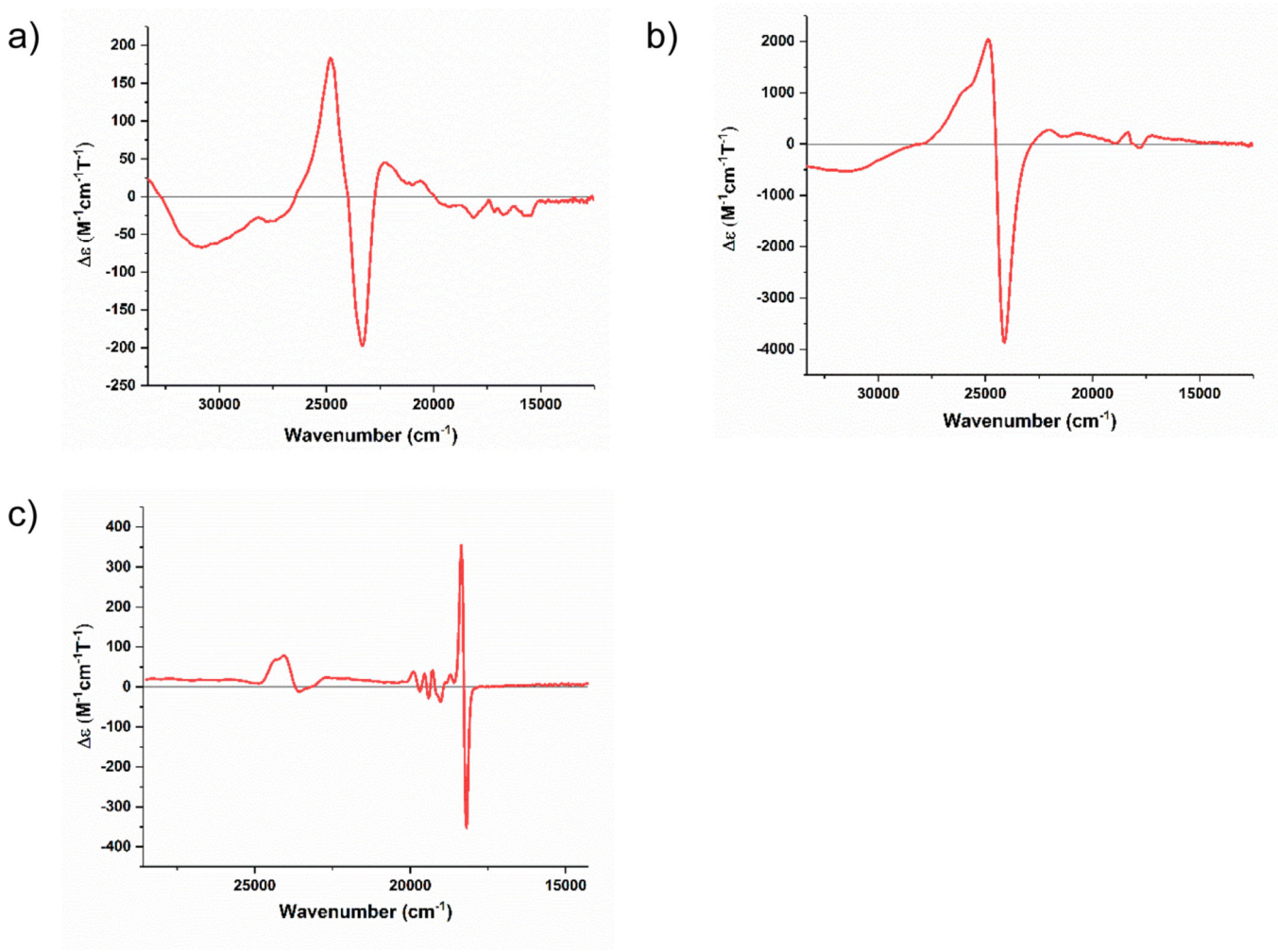

Figure 2.

Near-UV/visible-region MCD spectra of a) high-spin ferric horse heart myoglobin (10.6 μM), b) low-spin ferric horse heart Cytochrome *c* (2.9 μM) and c) low-spin ferrous Cytochrome *c* (2.3 μM). Each sample was prepared with ~50% glycerol in TIP7 buffer at pH 7. Spectra were recorded at 2 K.

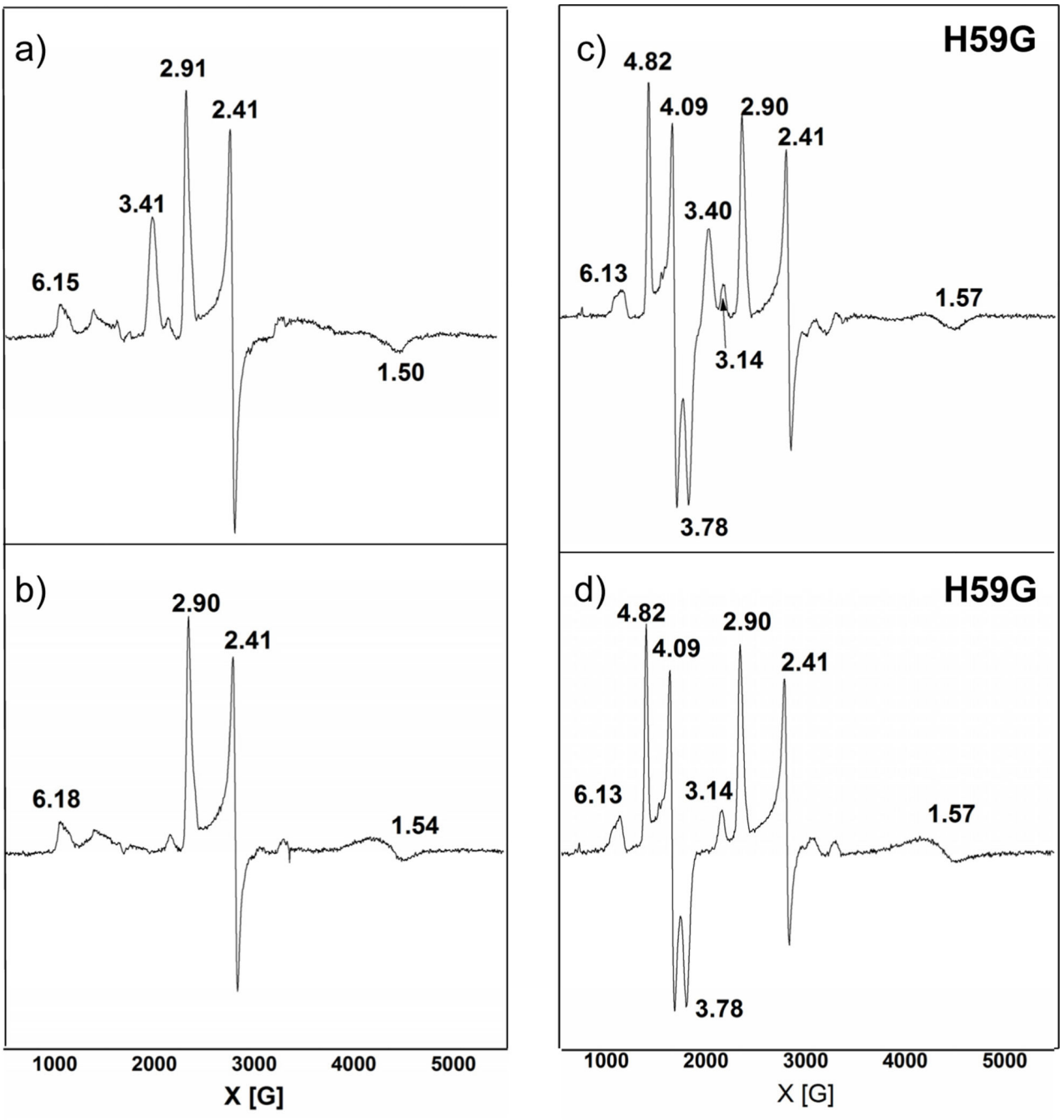

Figure 3.

EPR spectra of a) 420 μM diferric Ne*CcP*, b) 490 μM semi-reduced Ne*CcP*, c) 419 μM diferric *Ne*H59G CcP, and d) 460 μM semi-reduced *Ne*H59G CcP. Experiments were conducted at 9.27 GHz, a power of 20 mW, and a temperature of 12 K.

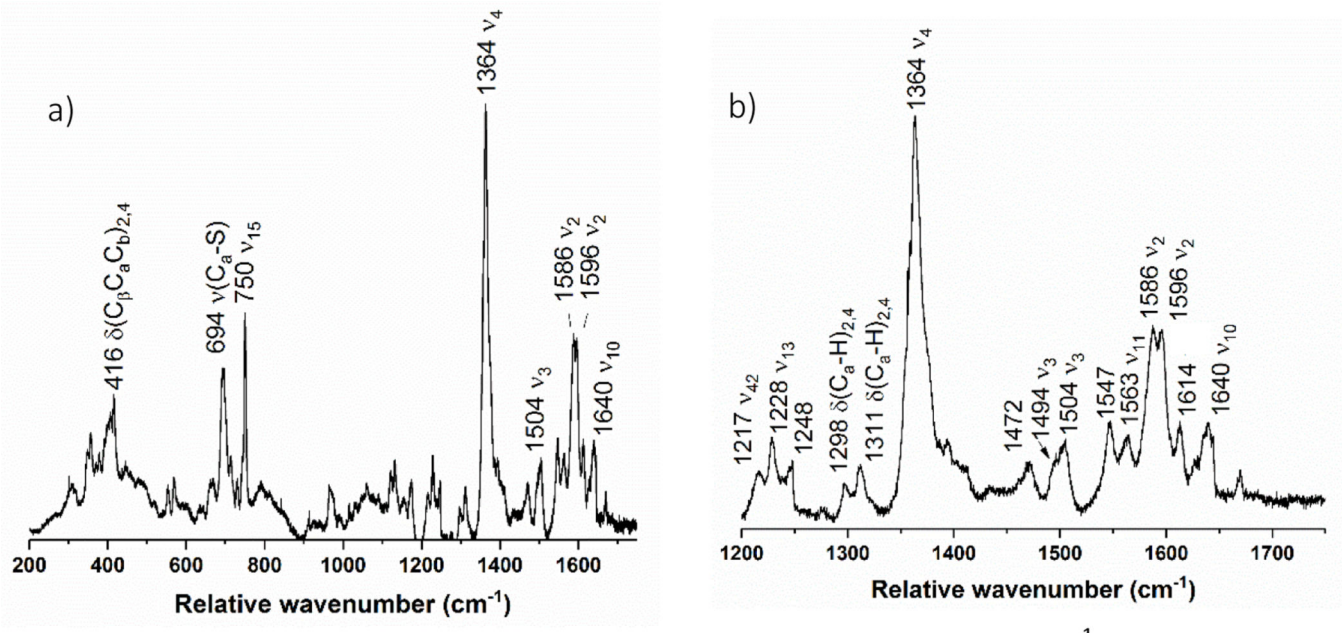

Figure 4.

Resonance Raman spectrum of diferric Ne*CcP* from a) 200 to 1750 cm^{-1}, and b) enlarged view of the 1200 to 1750 cm^{-1} region. The sample was 105 μM with 50% glycerol in pH 7 TIP7 buffer. The sample was excited at 413.1 nm using a Krypton ion gas laser.

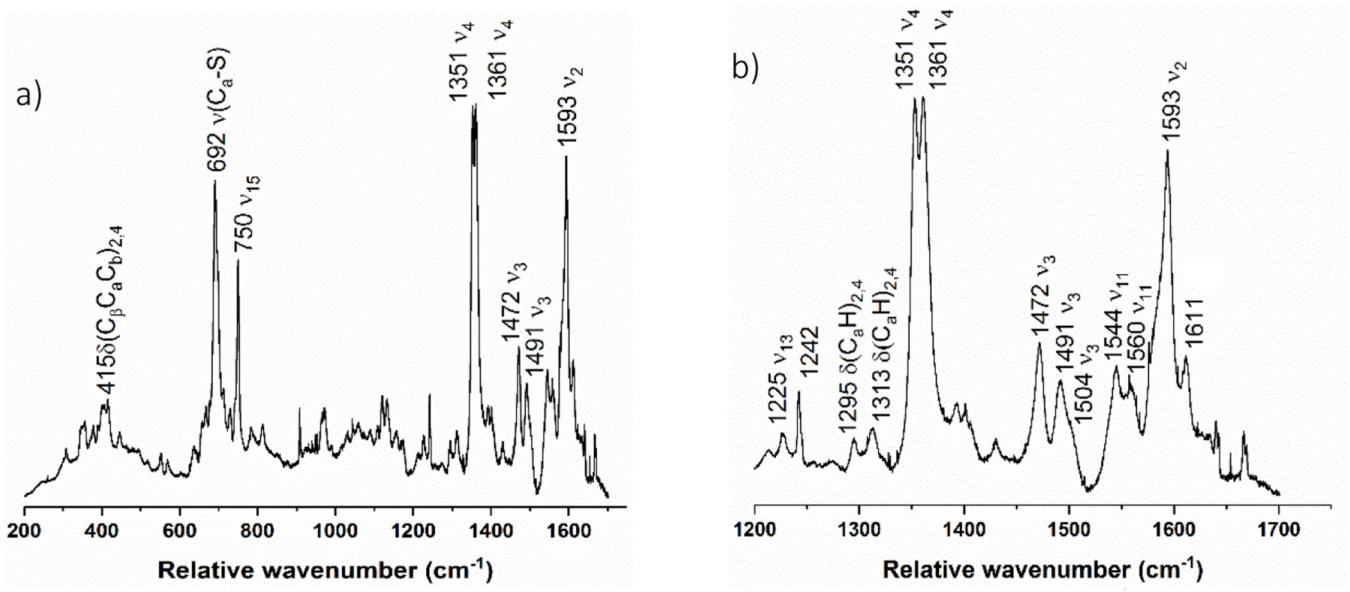

Figure 5.

Resonance Raman spectrum of semi-reduced *Ne*CcP from a) 200 to 1750 cm^{-1}, and b) enlarged view of the 1200 to 1750 cm^{-1} region. The sample was 160 μM with 50% glycerol in pH 7 TIP7 buffer. The sample was excited at 413.1 nm using a Krypton ion gas laser.

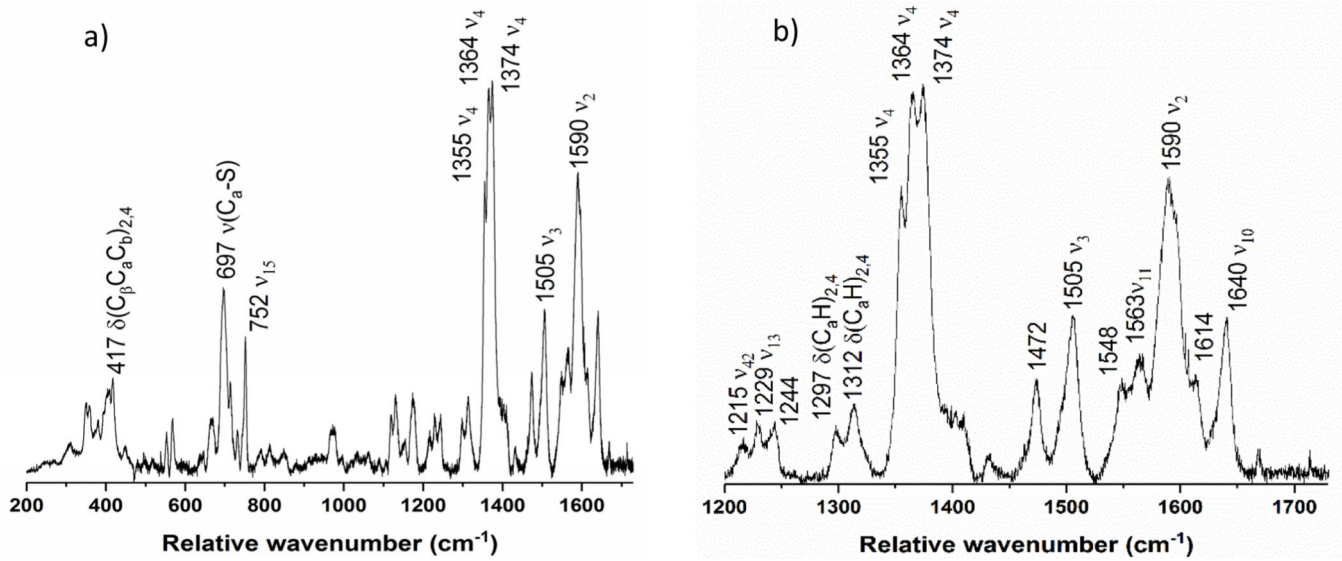

Figure 6.

Resonance Raman spectrum **diferric *Ne*H59G CcP** from a) 200 to 1750 cm^{-1}, and b) enlarged view of the 1200 to 1750 cm^{-1} region. The sample was 419 μM with 30% glycerol in pH 7 TIP7 buffer. The sample was excited at 413.1 nm using a Krypton ion gas laser at 77 K.

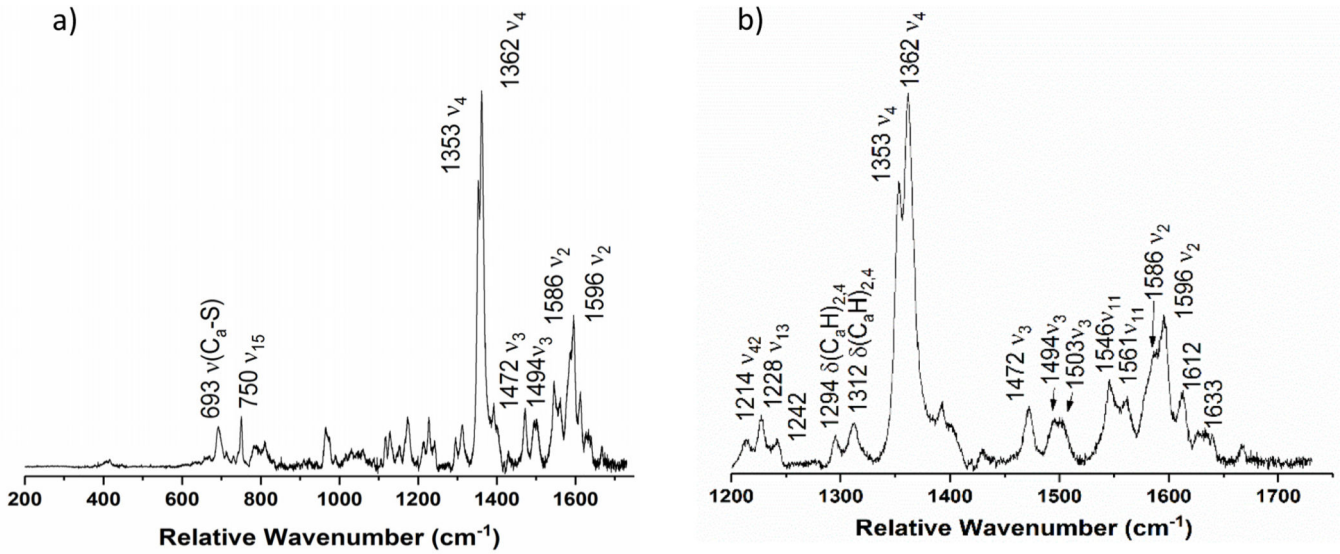

Figure 7.

Resonance Raman spectrum of **semi-reduced *Ne*H59G CcP** from a) 200 to 1750 cm^{-1}, and b) enlarged view of the 1200 to 1750 cm^{-1} region. The sample was 460 μM with 30% glycerol in pH 7 TIP7 buffer. The sample was excited at 413.1 nm using a Krypton ion gas laser at 77 K.

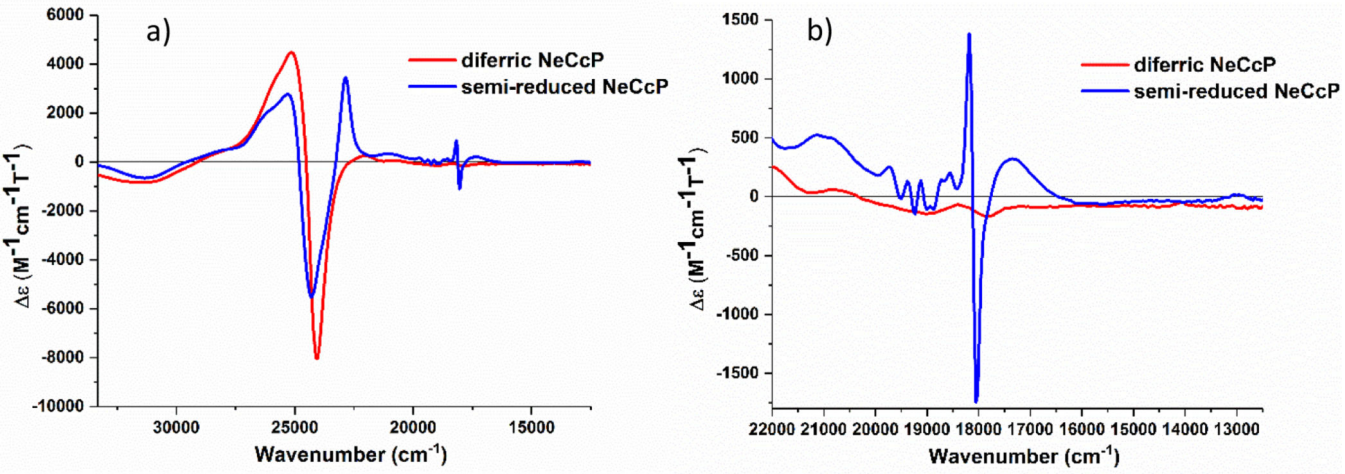

Figure 8.

a) Near-UV/visible-region MCD spectra of the diferric and semi-reduced states of *Ne*CcP, and b) a close-up of the Q-band region of the spectra. Samples were 20 μM with ~50% glycerol in a TIP7 buffer at pH 7. Spectra were recorded at 2 K.

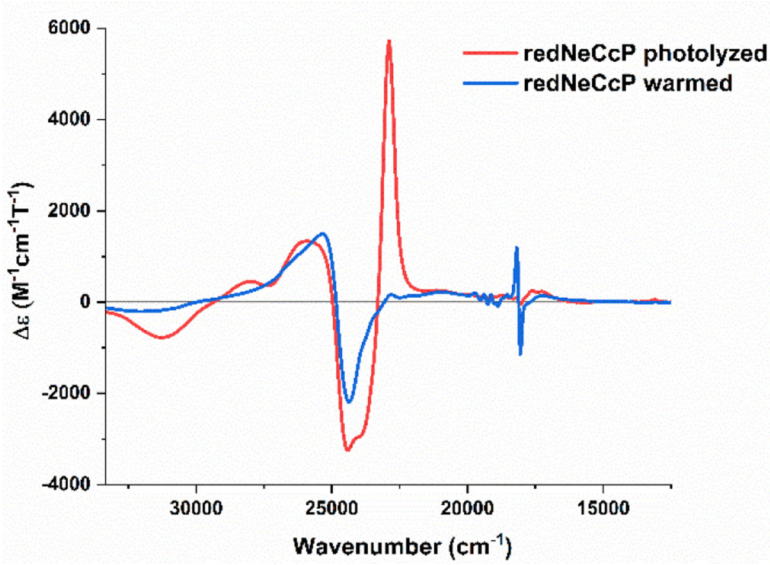

Figure 9.

Near-UV/visible-region MCD spectra of a semi-reduced Ne*CcP* sample that was photolyzed with a mercury lamp, and after warming the sample to 70 K in the dark and then cooling the sample back to 2 K. The sample was 3.1 μM with ~50% glycerol in a TIP7 buffer at pH 7. Spectra were recorded at 2 K.

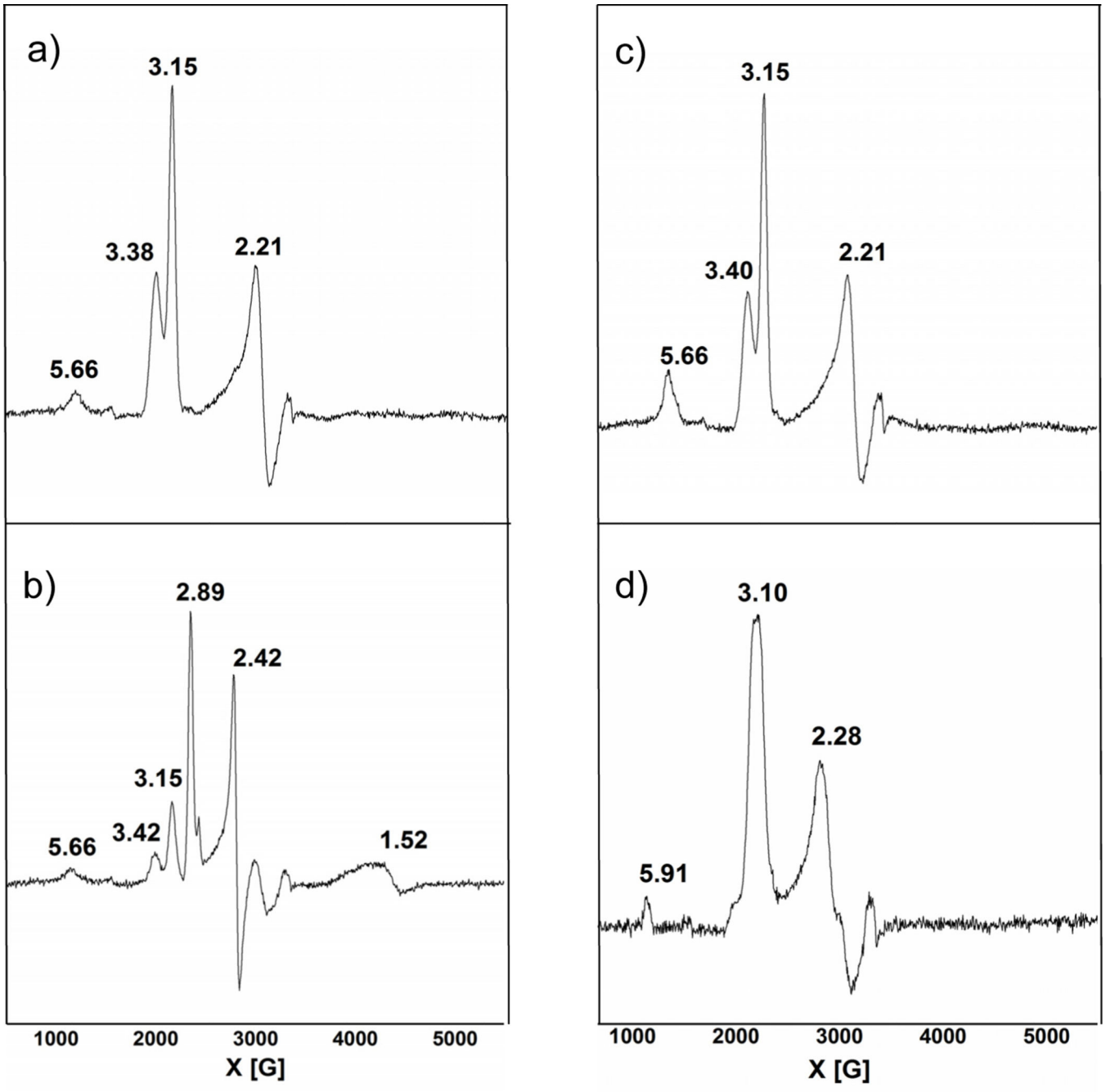

Figure 10.

EPR spectra of a) 330 diferric *So*CcP, b) 230 semi-reduced *So*CcP, c) 280 diferric *So*H80G CcP, and d) 340 μM semi-reduced *S0*H8OG CcP. Experiments were conducted at 9.27 GHz, a power of 20 mW, and a temperature of 12 K.

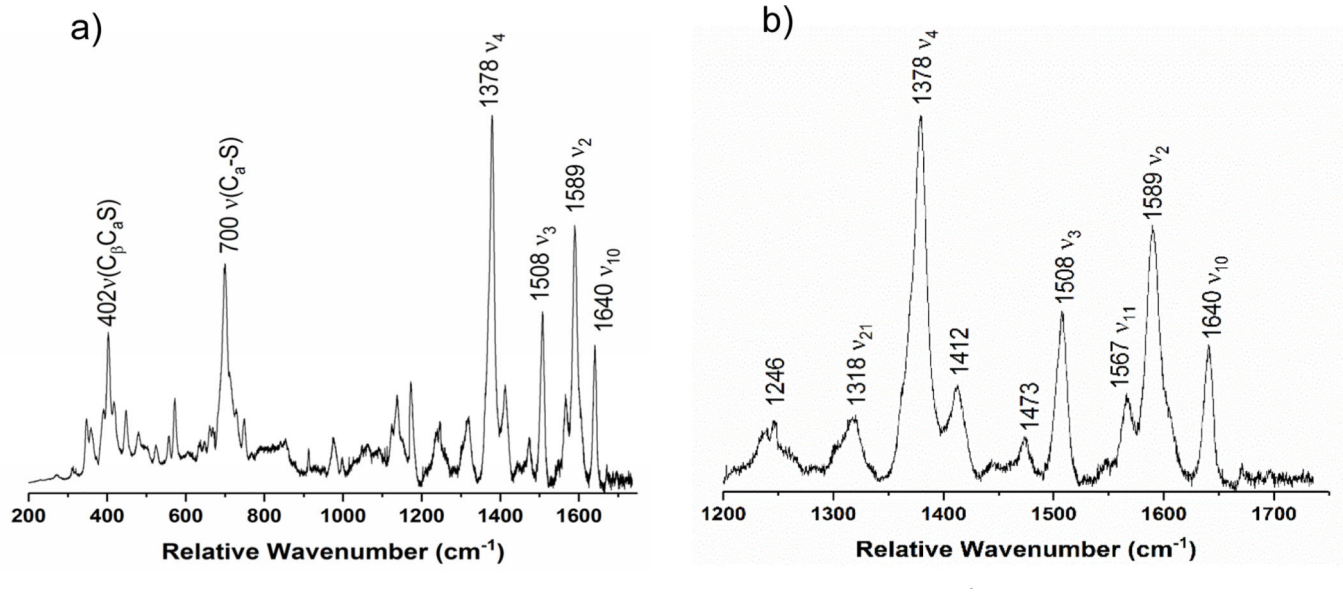

Figure 11.

Resonance Raman spectrum of **diferric SoCcP** from a) 200 to 1750 cm^{-1} and b) enlarged view of the 1200 to 1750 cm^{-1} region. The sample was 105 μM with 50% glycerol in pH 7 TIP7 buffer. The sample was excited at 413.1 nm using a Krypton ion gas laser at 77 K.

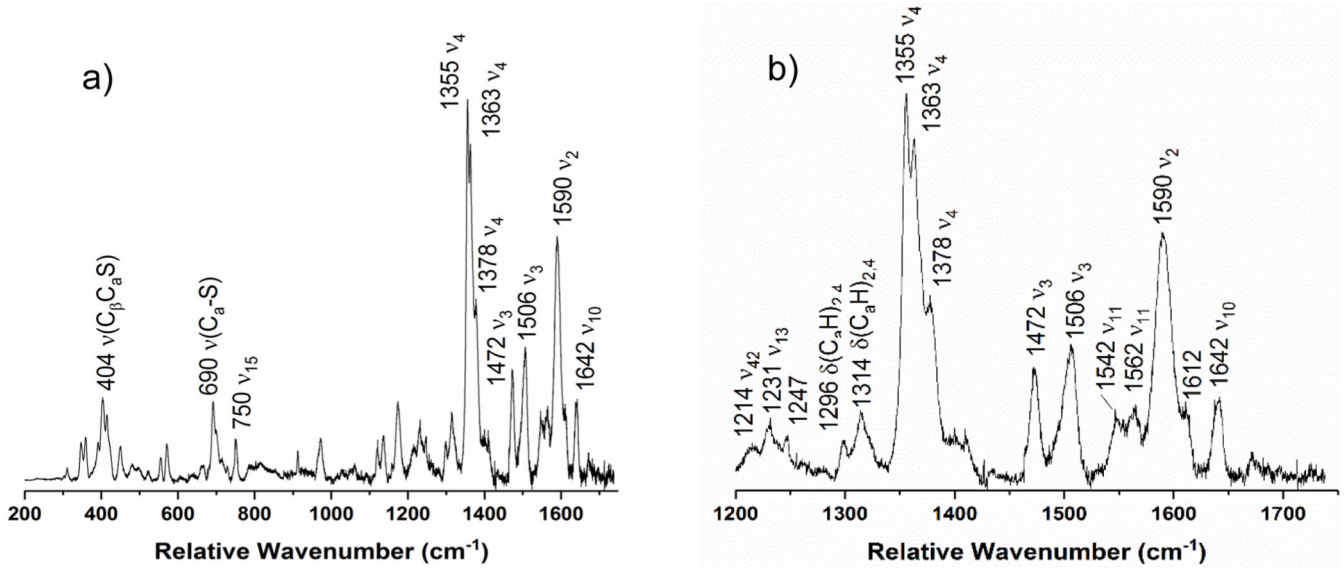

Figure 12.

Resonance Raman spectrum of **semi-reduced SoCcP** from a) 200 to 1750 cm^{-1} and b) enlarged view of the 1200 to 1750 cm^{-1} region. The sample was 160 μM with 50% glycerol in pH 7 TIP7 buffer. The sample was excited at 413.1 nm using a Krypton ion gas laser at 77 K.

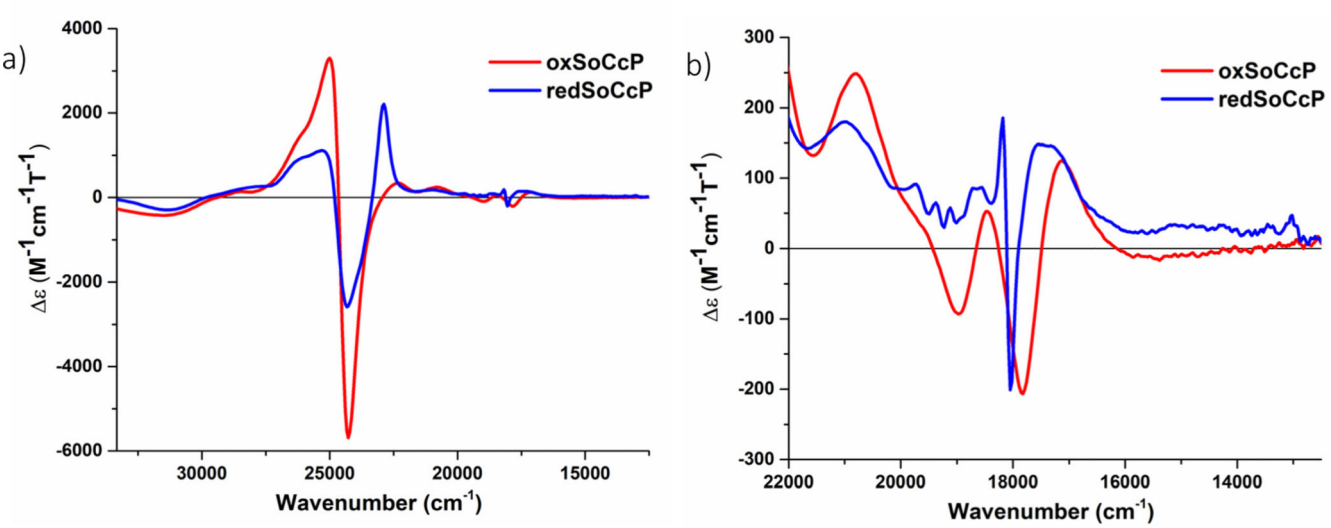

Figure 13.

a) Near-UV/visible-region MCD spectra of the diferric and semi-reduced states of *So*CcP and b) a close-up of the visible region of the spectra. The sample was 20 μM with ~50% glycerol in a TIP7 buffer at pH 7. Spectra were recorded at 2K.

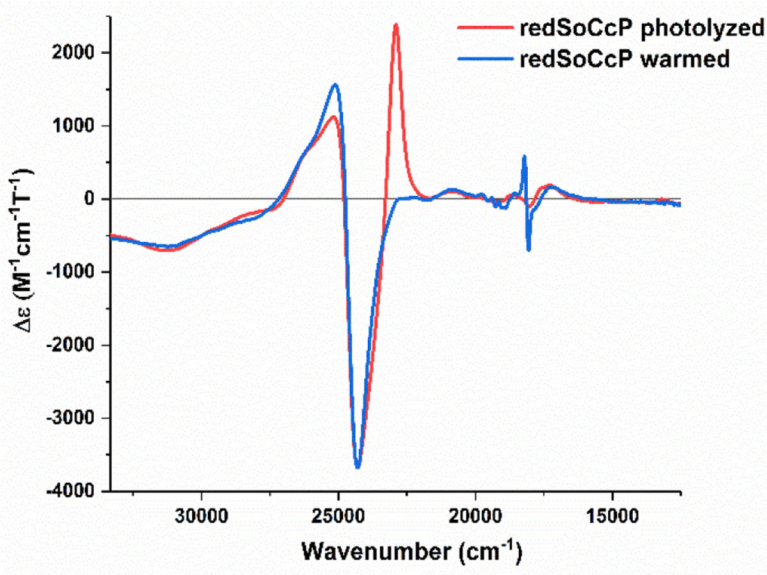

Figure 14.

Near-UV/visible-region MCD spectra of a semi-reduced *So*CcP sample that was photolyzed with a mercury lamp, and after warming the sample to 70 K in the dark and then cooling the sample back to 2 K. The sample was 2.0 μM with ~50% glycerol in a TIP7 buffer at pH 7. Spectra were recorded at 2 K.

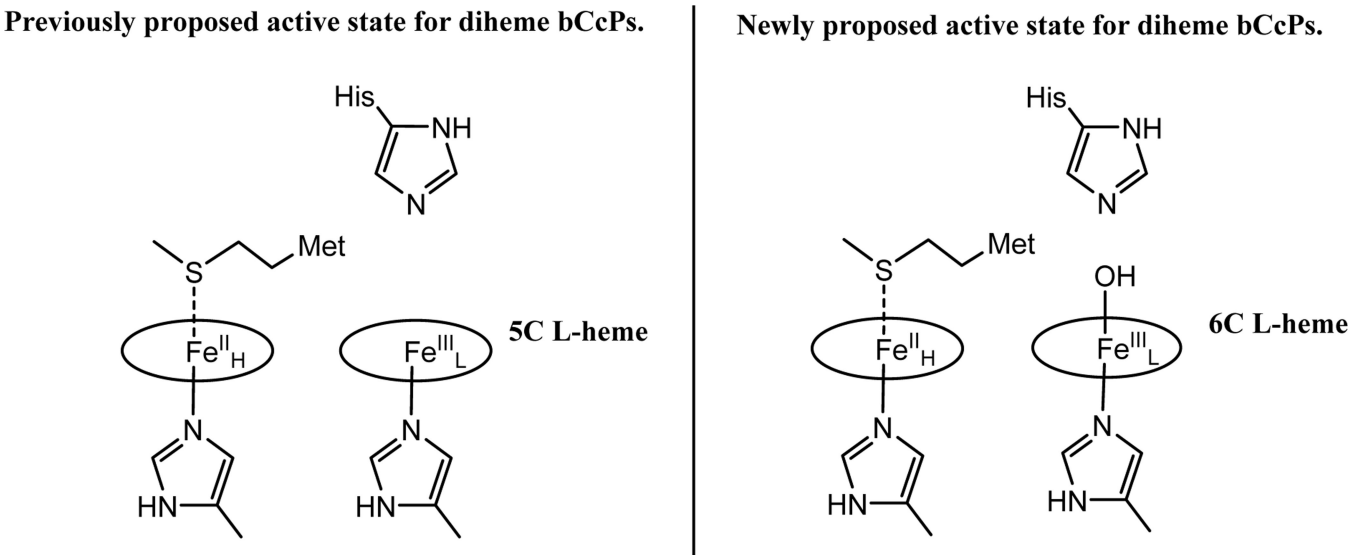

Figure 15.

The previously proposed active state for diheme bCcPs (left) and the newly proposed active state for these enzymes (right, this work).

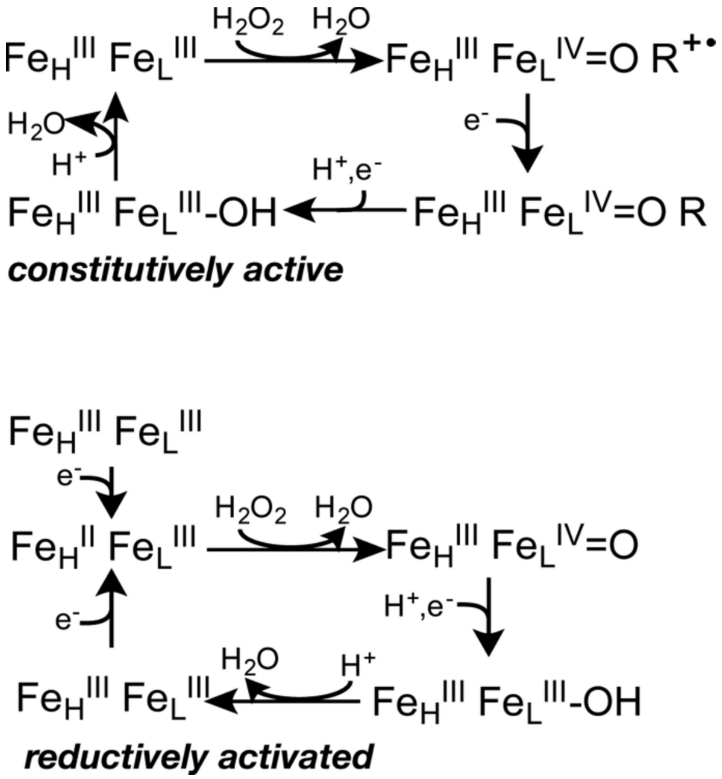

Scheme 1.

Proposed reaction mechanisms for constitutively active and activatable bCcPs (Modified from refs 20 and 21).

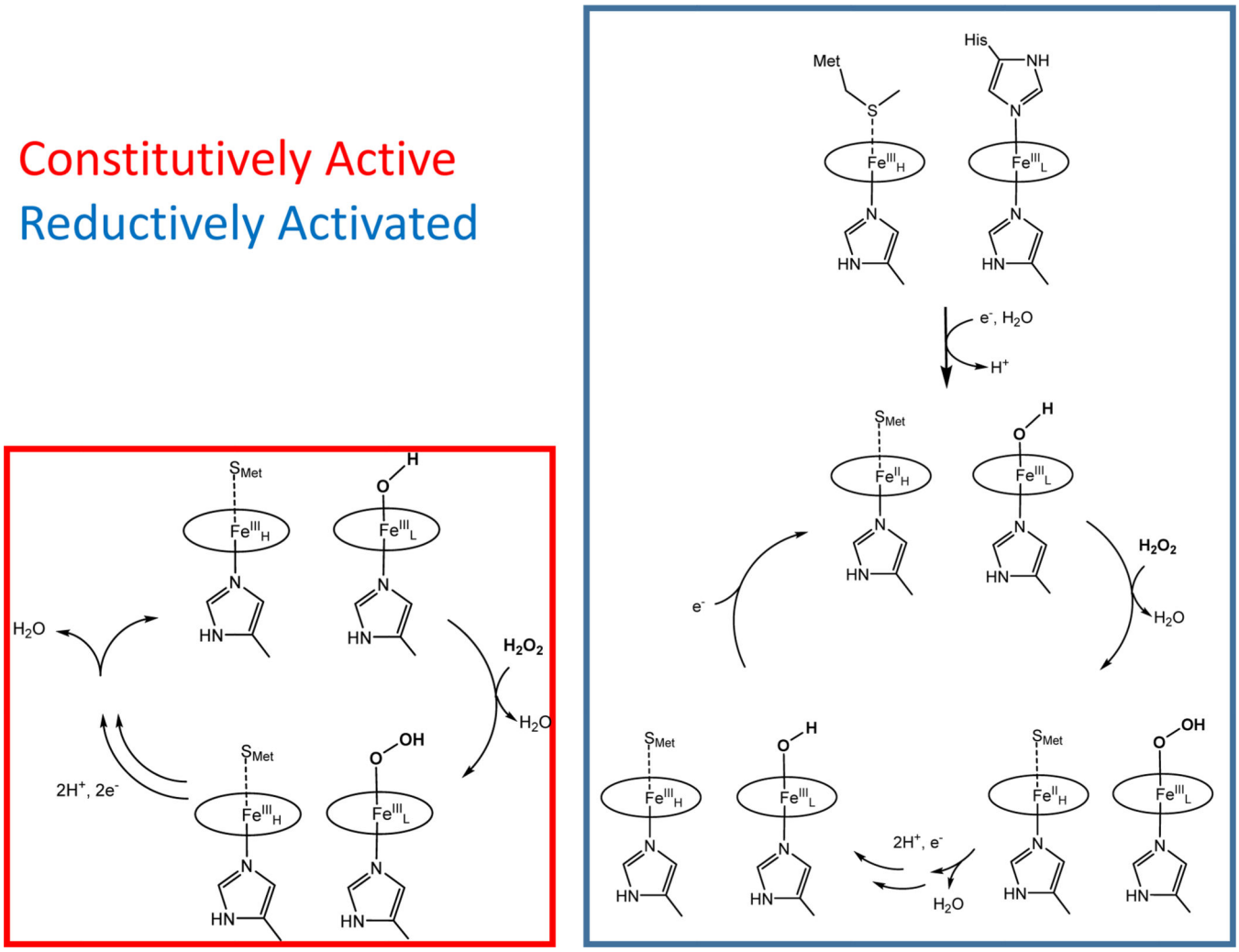

Scheme 2.

Possible mechanisms for constitutively active (left) and reductively activated (right) bCcP enzymes. The L-heme remains low-spin in each step of the mechanism prior to substrate binding. In the case of the reductively activated enzymes, EPR results suggest that a hydroxide is bound to the L-heme upon reduction of the H-heme.

Table 1.

Key spectroscopic results for the assignments of the H-heme and L-heme in *Ne*CcP.

Heme	Data	*Ne*CcP, DF	*Ne*CcP, SR
High potential, H-heme	Oxidation State	Ferric	Ferrous
	Spin State	LS	LS/HS[a]
	EPR data	g = 3.41	Disappearance of g = 3.41
	rRaman data	1364 (ν_4), 1504 (ν_3), 1640 (ν_{10})	1351 (ν_4), 1472 (ν_3), 1492 (ν_3)
	MCD data	25130 cm^{-1},24050 cm^{-1}	22860 cm^{-1}, 18160 cm^{-1}
Low-potential, L-heme	Oxidation State	Ferric	Ferric
	Spin State	LS	LS
	EPR data	g = 2.91, 2.41, 1.50	g = 2.90, 2.41, 1.54
	rRaman data	1364 (ν_4), 1504 (ν_3), 1640 (ν_{10}), no 1480 (ν_3)	1361 (ν_4), 1504 (ν_3), no 1480 (ν_3)
	MCD data	25130 cm^{-1},24050 cm^{-1}	25280 cm^{-1}, 24300 cm^{-1}

DF = diferric enzyme, SR = semi-reduced enzyme, LS = low-spin, HS = high-spin

[a] HS ferrous H-heme results from photolysis of the Fe-S_{met} bond

Table 2.

Key spectroscopic results for the assignments of the H-heme and L-heme in *So*CcP.

Heme	Data	*So*CcP, DF	*So*CcP, SR
High potential, H-heme	Oxidation State	Ferric	Ferrous
	Spin State	LS	LS/HS[a]
	EPR data	g = 3.38	Disappearance of g = 3.38
	rRaman data	1378 (v_4), 1508 (v_3), 1640 (v_{10})	1355 (v_4), 1472 (v_3)
	MCD data	25000 cm^{-1},24300 cm^{-1}	22880 cm^{-1}, 18160 cm^{-1}
Low-potential, L-heme	Oxidation State	Ferric	Ferric
	Spin State	LS	LS
	EPR data	g = 3.15, 2.21	g = 2.89, 2.42, 1.52
	rRaman data	1378 (v_4), 1508 (v_3), 1640 (v_{10}), no 1480 (v_3)	1363/1378 (v_4), 1506 (v_3), no 1480 (v_3)
	MCD data	25000 cm^{-1},24300 cm^{-1}	25280 cm^{-1}, 24310 cm^{-1}

DF = diferric enzyme, SR = semi-reduced enzyme, LS = low-spin, HS = high-spin

[a] HS ferrous H-heme results from photolysis of the Fe-S_{met} bond